EFDA–JET–PR(10)41

G. Giruzzi, M. Lennholm, A. Parkin, G. Aiello, M. Bellinger, J. Bird, F. Bouquey, H. Braune, A. Bruschi, P. Butcher, R. Clay, E. de la Luna, G. Denisov, T. Edlington, J. Fanthome, D. Farina, J. Farthing, L. Figini, S. Garavaglia, J. Garcia, M. Gardener, T. Gerbaud, G. Granucci, J. Hay, M. Henderson, S. Hotchin, V.N. Ilyin, M. Jennison, W. Kasparek, P. Khilar, N. Kirneva, D. Kislov, S. Knipe, A. Kuyanov, X. Litaudon, A.G. Litvak, A. Moro, S. Nowak, V. Parail, B. Plaum, G. Saibene, C. Sozzi, P. Späh, D. Strauss, E. Trukhina, A. Vaccaro, A. Vagdama, V. Vdovin and JET EFDA contributors

# Objectives, Physics Requirements and Conceptual Design of an ECRH System for JET

"This document is intended for publication in the open literature. It is made available on the understanding that it may not be further circulated and extracts or references may not be published prior to publication of the original when applicable, or without the consent of the Publications Officer, EFDA, Culham Science Centre, Abingdon, Oxon, OX14 3DB, UK."

"Enquiries about Copyright and reproduction should be addressed to the Publications Officer, EFDA, Culham Science Centre, Abingdon, Oxon, OX14 3DB, UK."

The contents of this preprint and all other JET EFDA Preprints and Conference Papers are available to view online free at www.iop.org/Jet. This site has full search facilities and e-mail alert options. The diagrams contained within the PDFs on this site are hyperlinked from the year 1996 onwards.

# Objectives, Physics Requirements and Conceptual Design of an ECRH System for JET

G. Giruzzi[1], M. Lennholm[2,3], A. Parkin[4], G. Aiello[5], M. Bellinger[4], J. Bird[4], F. Bouquey[1], H. Braune[6], A. Bruschi[7], P. Butcher[4], R. Clay[4], E. de la Luna[2,8], G. Denisov[9], T. Edlington[4], J. Fanthome[4], D. Farina[7], J. Farthing[4], L. Figini[7], S. Garavaglia[7], J. Garcia[1], M. Gardener[4], T. Gerbaud[10], G. Granucci[7], J. Hay[4], M. Henderson[11], S. Hotchin[4], V.N. Ilyin[12], M. Jennison[4], W. Kasparek[13], P. Khilar[4], N. Kirneva[12], D. Kislov[12], S. Knipe[4], A. Kuyanov[12], X. Litaudon[1], A.G. Litvak[9], A. Moro[7], S. Nowak[7], V. Parail[4], B. Plaum[13], G. Saibene[14], C. Sozzi[7], P. Späh[5], D. Strauss[5], E. Trukhina[12], A. Vaccaro[5], A. Vagdama[4], V. Vdovin[12]
and JET EFDA contributors*

***JET-EFDA, Culham Science Centre, OX14 3DB, Abingdon, UK***

*[1]CEA, IRFM, 13108 Saint-Paul-lez-Durance, France.*
*[2]EFDA Close Support Unit, Culham Science Centre, OX14 3DB, Abingdon, OXON, UK*
*[3]European Commission, B-1049 Brussels, Belgium*
*[4]EURATOM-CCFE Fusion Association, Culham Science Centre, OX14 3DB, Abingdon, OXON*
*[5]Karlsruhe Institute of Technology, D-76021 Karlsruhe, Germany*
*[6]Max-Planck-IPP, Euratom Association, D-17491 Greifswald, Germany*
*[7]Istituto di Fisica del Plasma CNR, Euratom Association, 20125 Milano, Italy*
*[8] Laboratorio Nacional de Fusion, Asoc. EURATOM-CIEMAT, 28040, Madrid, Spain*
*[9] Institute of Applied Physics, Nizhny Novgorod 603155, Russia*
*[10]LPTP, Ecole Polytechnique, 91128 Palaiseau, France*
*[11]ITER Organization, 13108 Saint-Paul-lez-Durance, France*
*[12]RRC 'Kurchatov Institute', Moscow, Russia*
*[13]Institut für Plasmaforschung der Universität Stuttgart, D-70569 Stuttgart, Germany*
*[14]Fusion for Energy, 08019 Barcelona, Spain*
** See annex of F. Romanelli et al, "Overview of JET Results", (23rd IAEA Fusion Energy Conference, Daejon, Republic of Korea (2010)).*

Preprint of Paper to be submitted for publication in
Nuclear Fusion

**ABSTRACT.**
A study has been conducted to evaluate the feasibility of installing an Electron Cyclotron heating and current drive system on the JET tokamak. The main functions of this system would be: electron heating, sawtooth control, Neoclassical Tearing Mode control to access high beta regimes and current profile control to access and maintain advanced plasma scenarios. This paper presents an overview of the studies performed in this framework by an EU-Russia project team. The motivations for this major upgrade of the JET heating systems and the required functions are discussed. The main results of the study are summarised. The usefulness of a 10MW level EC system for JET is definitely confirmed by the physics studies. Neither feasibility issues nor strong limitations for any of the functions envisaged have been found. This has led to a preliminary conceptual design of the system.

## 1. INTRODUCTION

The future JET programme [1], after the installation of the ITER-like wall [2], will be mainly focused on the consolidation of the physics basis of the three main ITER scenarios, i.e., the ELMy H-mode, the hybrid scenario and the advanced steady-state scenario [3]. In ITER, these scenarios will make substantial use of Electron Cyclotron (EC) waves, for heating as well as for control of both the MHD activity and the current density profile [4-6]. Electron Cyclotron Resonance Heating (ECRH) and Current Drive (ECCD) will play a special role in the operation of ITER, because it will be routinely involved, unlike the other heating and CD systems, in practically every phase of the ITER discharges. This situation is unprecedented, and the next decade this type of tokamak operation has to be seriously studied and documented in order to save time and money on a much more complex and costly device such as ITER. Therefore, a programme for preparation, validation and optimization of the ITER scenarios in present tokamaks would strongly benefit from, and even require, an ECRH/ECCD system. This gives a strong motivation for examining the feasibility of the construction and implementation of such a system in JET by 2014-2015, for an intensive exploitation before the start of ITER. The possibility of implementing an ECRH system on JET has already been considered in the past [7]. Those early studies were of course a good basis for a new feasibility analysis, however, changes in the general context and evolutions of motivations, physics and technology in this area had to be taken into account. Synergies with the development of the ITER ECRH system [8] have been systematically pursued.

This paper reports on the results of these feasibility studies for a JET ECRH system, carried out under bilateral agreement between the European Union and the Russian Federation. Both physics studies, aiming at a definition of the basic parameters of the system (wave frequency, launching geometry, power required), and exploration of the main technical options (wave generation and transmission, antenna design, power supply, auxiliaries, layout and port allocation, control systems, diagnostics) have been performed. A preliminary assessment of cost, time schedule, manpower and risks has been made. The plan of the paper is the following. Section 2 describes the basic procedure used to design an ECRH system for JET. Section 3 deals with physics requirement studies, including

description of the reference scenarios considered for future JET operation, wave propagation and absorption calculations, MHD control studies and full scenario simulations. The various system components are shortly described in Section 4, with particular attention to the most complex one, i.e., the antenna. Conclusions are drawn in Section 5.

## 2. RATIONALE FOR THE DESIGN OF AN ECRH SYSTEM.

EC waves, as a heating and CD tool, have a number of advantages and a few drawbacks. The main advantages are related to the strongly localised, controllable absorption; to the easy coupling, virtually independent of the plasma edge conditions; to the availability of high power sources and to the maturity of the wave transmission and launch technology. The main drawbacks are the sensitivity to the magnetic field, due to the resonant character of the interaction; the strong decrease of CD efficiency when the absorption moves off-axis, in particular on the low-field side, owing to trapped electrons; the effect of refraction and cut-off at high density – low wave frequency; the possibility of unwanted absorption at a higher harmonic of the resonant frequency (harmonic overlap). A careful design of an ECRH system should make use of the physical properties of the interaction in order to optimise the exploitation of the advantages, while limiting the impact of the drawbacks.

The main physics ingredients of the EC wave plasma interaction, to be used in the design, are:

- the resonance condition: $\omega = n\omega_{ce}(R) + k_{||} v_{||}$ (where $\omega = 2\pi f$, $\omega_{ce} = 2\pi f_{ce}$, and f, $f_{ce}$ are the wave frequency and the relativistic electron cyclotron frequency, R is the coordinate along the major radius, n is the harmonic number, $k_{||}$ and $v_{||}$ are the components of the wave vector and electron velocity parallel to the magnetic field)
- the Doppler effect (the $k_{||} v_{||}$ term in the resonance condition), which causes both shift and broadening of the absorption line
- the wave polarisation (X or O-mode), which determines the absorption rate (X and O stand for extraordinary and ordinary modes, respectively)
- the harmonic overlap: the separation between adjacent harmonic $\Delta w$ scales as $\Delta\omega/\omega \sim 1/n$; the absorption of the X-mode for $n > 1$ scales as $n_e T_e^{n-1}$, where ne and Te are the electron density and temperature.
- the CD efficiency (decreasing with the normalised flux coordinate r and increasing with the poloidal angle of the absorption point, measured from the equatorial plane – low-field side, because of trapped-electrons effects)
- the refraction effects (including the possibility of wave cut-off)
- the launching geometry (antenna location and injection angles)

The functions defined by the system objectives require mildly localised absorption and CD in the plasma core (normalised radius $\rho < 0.3$) and at mid-radius ($\rho \sim 0.5$-$0.6$), together with strongly localised CD at ($\rho \sim 0.6$-$0.75$) for Neoclassical Tearing Mode (NTM) stabilization. It is difficult to realize all these objectives, at various magnetic fields, with a single system. For instance, in the ITER ECRH

system [8] (that has to work essentially at a single value of the magnetic field) the functions have been split between two dedicated systems, working at the same wave frequency, but with completely different wave launch geometries: the Equatorial Launcher (with toroidal steering but fixed poloidal injection angles) is dedicated to the core functions, whereas the Upper Launcher (with poloidal steering but fixed toroidal injection angles) is dedicated to localised CD for NTM stabilization.

This type of problems would find a solution with multiple-frequency gyrotrons and broadband wave transmission systems. For the time being, only single or double frequency gyrotrons are reliable, and wave transmission for a two-frequency system is penalized by a significant complexity at the level of the windows. This implies that the first constraint on the design is the selection of the most relevant magnetic field range (or ranges) at which the system is bound to operate. This selection, connected with physics and programmatic considerations, must also take into account the availability of the wave sources, in order to end up with a magnetic field range compatible with existing sources and wave transmission technology.

Once a magnetic field is chosen, the ideal wave frequency is the one that yields a resonance located on the high-field side, at $\rho \sim 0.3-0.4$. In fact, in order to get central CD a toroidal angle has to be used, but this shifts the absorption towards the low-field side because of the Doppler effect. Therefore, a resonance on the high-field side results in core CD. This is illustrated by the ray-tracing plots of Fig.1 (left). Now, in this configuration the driven current can be simply shifted off-axis by tilting the poloidal injection, as shown in the same figure (middle plot). In both cases, the absorption is rather on the high-field side, where the trapped electron fraction is reduced, which optimises the CD efficiency. The absorption region is however broad (again because of the Doppler shift). Reducing the toroidal injection angle shifts the absorption closer to the resonance (thus further off-axis), while making it narrower, as shown in the right plot. This is exactly what is needed for the NTM control function.

Furthermore, the refraction effects must be checked, for a given frequency/polarisation combination, by ray-tracing calculations, together with the harmonic overlap. Note that spurious absorption at the upper harmonic should in most cases be avoided because i) it turns out to be broadly distributed, ii) the current is either driven in the opposite direction with respect to the main harmonic, or driven in the same direction (because of the Ohkawa effect), but with very poor efficiency. In the following, the practical criterion that the upper harmonic absorption should be less than 10 % will be used.

## 3. PHYSICS REQUIREMENTS STUDIES

The main functions of an ECRH system on JET can be summarized as follows:

i) Central electron heating – to equilibrate electron and ion temperature, to scan the electron/ion power share up to ITER relevant values and to control impurities.

ii) Current profile control – to improve the performance and stationarity of advanced and hybrid scenarios.

iii) Sawtooth control – to shorten sawteeth through local current drive near the q = 1 surface and hence avoid triggering NTMs.
iv) NTM suppression through local current drive at the relevant rational q surface.

These objectives were translated into the requirement to heat the plasma or drive currents at various plasma minor radii. In order to fulfil all the objectives, the system should be able to deposit the ECRH power over almost the full range of plasma minor radii. For MHD control, the width of the deposition profile is also an important parameter. As the ECRH power is absorbed at or near the EC resonance, the physics objectives can only be fulfilled for a selected range of toroidal magnetic fields. Several state-of-the-art codes have been used to perform these studies, in particular the beam-tracing code GRAY [9] and the integrated modelling suite CRONOS [10].

### *3.1 REFERENCE SCENARIOS.*

Two recent JET discharges, both with parameters compatible with the ITER-like wall, have been identified and chosen as reference discharges for the simulations: Pulse No's: 73344 (for H-mode and hybrid scenarios) and 77895 (for advanced scenarios). The basic parameters of the discharges measured during the high performance phase are given in Table 1. These two experiments have very similar magnetic configuration at the separatrix characterized, in particular, by a high ITER like triangularity ($\delta \sim 0.4$) and with the outer strike point on the load bearing septum replacement plate (see Fig.2). These configurations are expected to be used routinely after the enhancement of the plasma facing components on JET: the ITER-like wall project [2]. Contrary to the inductive scenario (Pulse No: 73344), the advanced regime operates at high normalized pressure ($\beta_P \sim 1.5$ and $\beta_N \sim 2.8$) with a large Shafranov shift and with a broad qprofile ($q_{min} \sim 2$) characterized by a low value of internal inductance leading to a different distribution of the magnetic flux surfaces inside the plasma.

The time evolution of the applied power and the main plasma parameters together with the temperatures and electron density profiles are shown on Figs. 3 and 4 for the Pulse No's: 73344 and 77895, respectively. Mainly NBI (Neutral Beam Injection) power is applied on a relaxed q-profile ($q_0 \sim 1$) without any prelude phase for the Pulse No: 73344. On the contrary, in Pulse No: 77895, a combination of $P_{NBI} \approx 22$MW, $P_{ICRH} \approx 7$ MW and $P_{LHCD} \approx 2$ MW is applied just after a prelude phase in plasmas with weak magnetic shear and $q_0 \sim 2$ (full bore magnetic configuration during the current ramp-up). In view of using and studying the full capability of the heating and current drive mix in JET, these advanced scenario experiments rely on optimising the edge for good RF coupling while maintaining good core and edge confinement. Cold gas injection has been used to mitigate the impact of the ELMs on the core confinement, by reducing the ELMs size and penetration depth into the plasma core. In terms of electron density and temperatures profiles these selected examples display significant and very different characteristics, i.e.,

(i) for the Pulse No: 73344, a low electron temperature ($T_{e0} \sim 4$keV) but a high density ($n_{e0} \sim 8\times10^{19}m^{-3}$, $n_{e\text{-}ped} \sim 7\times10^{19}m^{-3}$) with a modest peaking density factor $n_{eo}/n_{e\text{-}ped} \sim 1.25$

(ii) on the contrary, the Pulse No: 77895 exhibits a much higher electron temperature (~8keV) at lower density ($n_{e0} \sim 6\times10^{19}m^{-3}$, $n_{e\text{-}ped} \sim 4\times10^{19}m^{-3}$) for maximizing the external non-inductive current drive together with a higher peaking factor $n_{eo}/n_{e\text{-}ped}$ ~1.6. The ion temperature has a strong Internal Transport Barrier (ITB).

### *3.2 WAVE PROPAGATION AND ABSORPTION.*

The first aim of the study was to determine the best choice of operating frequency [11].
Two gyrotron options were considered:

1) dual frequency gyrotrons (113GHz, 150GHz) as used on ASDEX Upgrade (105-140 GHz) with minor modification to increase the frequency;

2) 170GHz gyrotrons, as those developed for ITER.

The choice of the optimal frequency depends both on the range of magnetic field at which JET is expected to operate, and on the physics objectives of the project itself, i.e., the radial region in which EC plasma interaction must take place. At lowest order, the EC features can be identified by means of Fig.5, which shows the cyclotron frequency versus the major radius co-ordinate for different values of the vacuum central magnetic field $B_0$ in the range 2.4T–3.4T, and for the first, second and third cyclotron harmonics. In first approximation, EC waves interaction requires the cold resonance condition $f = nf_{ce}$ to be satisfied within the plasma ($2m < R < 3.8m$), although in case of oblique injection from the low field side the EC power may be fully absorbed before reaching the cold resonance located at Rce, i.e., at major radii $R > Rce$, especially in the case of large electron temperatures.

The following observations can be made from the plot. At 113GHz, first harmonic interaction occurs in the high field side for $B_0 > 2.8T$, while second harmonic occurs in the low field side for $B_0 < 2.6T$. Interaction occurs at second harmonic both at 150 and 170GHz in the whole magnetic field range, and, at a given field, in inner regions at 170GHz. Third harmonic absorption may affect the EC efficiency for $B_0 < 2.8T$ at 170GHz, if the electron temperature is large enough. For $B_0 > 3T$, interaction occurs in the low field side, thus reducing the current drive efficiency, due to trapped particle effects.

EC waves are to be injected polarized as Ordinary Mode (OM) in the case of first harmonic at 113GHz, and as eXtraordinary Mode (XM) in the case of second harmonic at 150, 170GHz. In fact, in some particular cases at high temperature, O-mode absorption at the second harmonic can also be used. The cut-off densities at the three frequencies are given in Table 2. Note that in case of XM the cut-off density depends on $N_{\|} = \sin\phi$, being $90° - \phi$ the angle between the wave-vector and the magnetic field. The cut-off density is found to be larger than $10^{20}\ m^{-3}$ for most cases of interest in oblique injection, so that refraction effects are not expected to play a major role, except in a few specific conditions.

Calculations have been performed using the GRAY code [9], a quasi-optical beam tracing code

for EC propagation. Power absorption is computed solving the relativistic dispersion relation for EC waves, taking into account high order terms in the Larmor radius expansion and higher harmonics contributions, while current drive is computed via the adjoint method. The calculations are performed in a linear framework, which is expected to be applicable for the EC power densities foreseen at JET.

For sake of simplicity, it is assumed that the EC beams are launched from two mirrors, with the same radial and two different vertical positions, corresponding to an upper and a lower location, $R = 4.3$m, $z = \pm 0.345$m. A divergent beam with waist $w_0 = 3$cm at the mirror has been considered. Note that the Upper Mirror (UM) is located slightly above the equatorial plane ($\Delta z \approx 10.5$cm), the magnetic axis being at $R = 3.04$ m, $z = 0.239$m, while the Lower Mirror (LM) is well below the equatorial plane ($\Delta z \approx -58.5$cm). The poloidal and toroidal injection angles a and b are defined in terms of the refractive index components as

$$N_R = -\cos\alpha\cos\beta, \quad N_\phi = \sin\beta, \quad N_z = -\sin\alpha\cos\beta \tag{1}$$

The angles $\alpha$ and $\beta$ are varied in a wide range, $-40° \le \alpha \le 40°$, and $0° \le \beta \le 26°$, with $\beta$ positive in order to drive a co-current. Note that a positive corresponds to negative $N_z$, i.e., to downwards injection.

The study produced a comprehensive evaluation of the minor radii accessible as a function of toroidal field for the two options. The results showed that the 113GHz, 150GHz option allowed good performance for toroidal fields below 2.7 T (2nd harmonic X mode at 150GHz) and for fields above 3.3T (fundamental O mode at 113GHz) while operation around 3T would be difficult with this frequency choice. Choosing 170GHz (2nd harmonic, X mode) would on the other hand allow excellent performance in the interval 2.7-3.1T with off axis current drive available in a significantly wider range. An example of the extensive calculations that were carried out (described in detail in [11]) is shown in Fig.6. The point clouds correspond to a full scan of the toroidal and poloidal injection angles for both reference scenarios and 170GHz. Each point represents the driven current per MW of injected wave power at a given combination of toroidal and poloidal angles, plotted as a function of the radial location of the maximum absorption (here and afterwards, the radial coordinate is the square root of the normalised toroidal magnetic flux). This type of plot clearly displays the plasma regions in which currents can be driven. Note the much higher CD efficiency obtained in the advanced scenario (associated with the higher temperature) and the differences between injection from the upper and the lower mirror, which is determined by the different level of spurious absorption at the 3rd cyclotron harmonic [11].

Full angular scans of this type have been repeated at various magnetic fields for both the H-mode and the advanced scenarios, with an appropriate rescaling of current, density and temperature, as described in [11]. The performances for the H-mode scenario are summarized in Fig.7 by means of a traffic light colour code, which refers to the main physics applications of the ECRH in JET. The colour code is assigned to each physics application on the basis of the driven current per unit power,

excluding cases of poor absorption or too strong 3rd harmonic absorption. Figure 7 illustrates the parameter space at which 170GHz waves can be used in JET for the H-mode scenario. For advanced scenarios, a very similar pattern is obtained, but shifted at 0.1-0.2 T higher magnetic fields.

In conclusion, as a consequence of these calculations, 170 GHz has been taken as the reference value of the wave frequency for the rest of the study. With this choice of gyrotron frequency the injection angles required to fulfil the objectives were found to be: toroidal: $-25°$ to $+25°$ , poloidal range: 30° around an appropriate mean value, depending on the precise mirror locations.

### *3.3 NTM STABILISATION.*

Use of localised ECCD for stabilisation of (3,2) and (2,1) modes, has been considered a key function for the access to high b, in particular in H-mode scenarios [12]. The beamtracing results have been used in connection with the generalised Rutherford equation [13] to study the evolution of the magnetic island width in the presence of ECCD.

The stability of the (2,1) and (3.2) NTM modes is investigated for the H-mode scenario of the JET reference Pulse No: 73344 at $t \sim 21$s (see Sec.3.1) for EC power at 170GHz, continuously injected (i.e., no power modulation is considered) from 2 mirrors at $z = 0.345$m (Upper Mirror-UM) and $z = -0.345$m (Lower Mirror-LM). The main plasma parameters used in the generalised Rutherford equation are listed in Table 3, where $\psi$ is the normalized flux function, $\rho_{t,p}$ the normalized radii in toroidal and poloidal flux co-ordinates, respectively; $\varepsilon$ is the local inverse aspect ratio, rs is the resonance surface location, $L_{q,p}$ are the local safety factor and pressure gradient lengths, $\beta_p$ is the local value of the poloidal beta. These and the other parameters entering the Rutherford equation have been chosen in agreement with the measured quantities of the 73344 discharge. The modes can evolve from an initial seed island to their saturated sizes when the local poloidal beta is larger than a minimum marginal critical value bp,cr, corresponding to the marginal island width wmar below which the NTMs are unconditionally stable. The stabilization criterion is to reduce the mode to its marginal width through the balance of the heating and current drive terms with all the other terms in the generalised Rutherford equation. In Fig.8 an example is given of the island width reduced to its marginal size for the (2,1) mode. Two cases are illustrated, with and without the ion current polarisation term $\Delta'_{pol}$ [14] in the Rutherford's equation. The polarization term shifts the threshold width as well as the marginal width to larger values with respect to those calculated without this term. Its stabilizing effect is much stronger if the mode frequency increases : rotation is beneficial for stabilization and can be a tool to avoid NTM onset. In JET NBI heated plasmas the modes are often rotating with frequency up to 10kHz for (2,1) and 20kHz for (3,2) as in the 73344 discharge, where the islands are at their marginal value.

Full scans of the toroidal injection angle and the magnetic field have been performed, every time adjusting the poloidal angles in order to obtain CD at the locations of the $q = 2$ and $q = 3/2$ resonant surfaces. The optimum toroidal injection angle is typically found in the range $10° - 15°$. The most critical quantity is the radial width of the driven current dcd, here defined as the full width of the

driven current density profile at e-1. This is in principle given by the beam tracing calculations presented in Sec.3.2, however, whenever the EC power required is > 1MW, the stabilising effect will be provided by the superposing several wave beams. The superposition will generally not be perfect and it will be difficult to keep it optimised in real time. Therefore, calculations have been performed using both the dcd computed by the beamtracing code (typically, ≤ 5cm) and different values of $\delta_{cd}$ treated as a free parameter. Results for both modes are summarised in Fig.9, where the stabilising EC power is plotted as a function of the magnetic field, for the optimum value of the injection angle $\beta$ (in general, different for each value of $B_0$). The dashed line corresponds to the dcd obtained from the beam tracing. The solid lines correspond to 2 values of $\delta_{cd}$ : 0.05m and 0.1m. Less than 6MW are predicted to stabilise the (3,2) mode at any magnetic field, while more than 8MW are required to control the (2,1) mode at $B_0 > 2.8$T, for a current channel width $\delta_{cd} = 0.1$m. At high fields, the (2,1) mode stabilisation becomes marginal because of the poor CD efficiency due to trapping effects: this is related to the fact that the cold EC resonance surfaces moves further and further to the low field side as the magnetic field increases (see Fig.5). Similar calculations performed for the advanced scenario give much more favourable results, owingto the higher driven currents associated to the higher $T_e/n_e$ ratio. Power modulation can still be used to improve the stabilisation efficiency; nevertheless, at the typical mode rotation frequency found in JET plasmas under condition of strong NBI heating (≥ 10kHz), this imposes stringent conditions on the power supplies, as discussed in Sec. 4.4.

### *3.4 SAWTOOTH CONTROL.*

ECCD application for sawtooth control looks promising because of excellent localisation of the heating power deposition and the possibility to control the power deposition location using steerable mirrors. ECCD in the vicinity of the q = 1 surface was shown to be a powerful tool to modify the sawtooth period in a number of experiments (e.g., [15-17]). Stabilising or destabilising effects were found to depend strongly on the location of the power deposition with respect to the q= 1 surface. The current density rather than the total value of the driven current was found to be crucial in the experiments in TCV and T-10 [15-16]. Dependence of the effect on the width of the EC driven current profile has been observed also in Asdex Upgrade experiments with NBI heating [17]. Real time control in the presence of stabilisation by fast particles, i.e., the typical ITER and JET situation, has been demonstrated in Tore Supra [18-19].

Beam tracing calculations combined with ASTRA transport simulations [20] and the Porcelli model [21] have been used to estimate the power required in order to have a significant impact on the sawtooth period for the H-mode scenario in JET. According to the Porcelli model, the sawtooth crash occurs when one of the following critical conditions is satisfied:

(2)

(3)

(4)

where the precise definitions of the various quantities appearing in Eqs. (2-4) can be found in [21].

The sawtooth crash model with critical conditions (2-4) was incorporated into the ASTRA code. The numerical factor c* has been taken equal to 0.5 as in [22]. The fast particle component ($\delta W_{fast}$) of $\delta\hat{W}$ has been calculated by the analytical formula used in [23]:

(5)

where $s_1$ is the shear at the $q = 1$ surface, located at $r = r^1$, and $\beta_{fast}$, $p_{fast}$ are the fast ions beta and pressure, respectively. The contribution of beam ions $\delta W_{fast}$ was calculated using the beam energy density taken from JETTO [24] simulations. The numerical factor cf has been taken equal to 0.4 in order to match the experimental value of the sawtooth period.

According to the results of the modelling, injection of $P_{ECH} = 2.5$MW should be sufficient for reduction of sawtooth period by a factor of ≥2 with counter-ECCD in the range of toroidal field $B_0 = 2.7$-$3.1$T for the conditions of the 73344 discharge. As an example, ASTRA evolution of the various terms involved in the sawtooth stability criteria (2-4) for $P_{EC} = 2.5$MW, $\varphi_t = 7°$, $\varphi_p = 0°$, $B_0 = 2.7$T, counter-ECCD, optimised power deposition, is shown in Fig. 10: after application of the EC power at t = 3.5s, a reduction of the sawtooth period by a factor of »2.5 has been attained. Co-ECCD has been found to be less effective than counter-ECCD for reduction of sawtooth period for sufficiently narrow profile of the driven current (wcd£0.05, in normalised radius co-ordinate). Thus, reduction of sawtooth period by a factor of »1.7 has been observed in the calculations for optimized power deposition for $P_{EC} = 2.5$MW, $\varphi_t = 7°$, $\varphi_p = 0°$, $B_0 = 2.7$T but co-ECCD. According to the results of the modelling, reduction of the sawtooth period by a factor of 2 in co-ECCD case can be achieved for $P_{EC} = 2.5$MW only in the most favourable geometry. Higher EC power (about $P_{EC} = 5$MW) is required to obtain sawtooth period reduction by a factor of 2 with co-ECCD in other spatial cases. We note that it looks problematic to attain reduction of sawtooth period by a factor of 2 for a wide profile of the driven current (with $w_{cd} > 0.07$) both in co and counter cases. This is illustrated in Fig.11, summarising the results of several ASTRA runs in which the EC power deposition location has been varied for both co- and counter-ECCD and two different values of the driven current width, while keeping the CD efficiency fixed. For sawtooth as for NTM control, optimisation of the antenna design is an essential step in order to keep the power deposition in the plasma as narrow as possible.

### *3.5 INTEGRATED MODELLING OF JET SCENARIOS WITH EC WAVES.*

The extensive beam-tracing calculations described in Sec.3.2 are the basis for a choice of the most

appropriate wave parameters corresponding to the various applications foreseen for the ECRH system on JET: wave frequency, antenna location, injection angles. The crucial parameter that remains to be estimated is of course the wave power required for the various functions. For some particular choices of the wave frequency and injection angles, MHD calculations have been performed in Sec.3.3 and 3.4, in order to estimate the power required to control NTM modes and sawteeth, respectively. The purpose of this Section is to evaluate the wave power impact on the scenarios that can be realised with the help of ECCD, in particular,

1) the EC power required for central electron heating, in order to equilibrate the electron and ion temperatures, mainly in the H-mode scenario
2) the EC power required for a substantial modification of the q profile, with applications to advanced and hybrid scenarios.

In order to perform these calculations, the plasma response to the application of EC waves has to be computed, i.e., the effect on temperature and current at least (although effects on density and Zeff should, in principle, also be considered). This requires a transport code with appropriate sources and sinks, i.e., an integrated modelling code. This work has been mainly performed by means of the CRONOS suite of codes [10], but simulations for the Hmode scenario were at first performed by JETTO [24] and were used as a basis for the best choice of the transport model.

The CRONOS code [10] solves the transport equations for various plasma fluid quantities (only current and temperatures in these simulations). This is done in one dimension (the toroidal magnetic flux coordinate associated with the minor radius), self-consistently with 2-dimensional magnetic equilibrium. CRONOS has been used for integrated modelling of full JET scenarios. Both interpretative and predictive simulations of the reference discharges have been performed, in order to test the predictive capability of the code with respect to current and temperature profiles. An example of these tests is shown in Fig. 12, i.e., a comparison of (smooth fits of) experimental electron and ion temperature profiles and the result of predictive simulations using the Bohm/gyro-Bohm transport model [25], for the JET Pulse No: 73344 (see Table 1, Fig.3). The agreement is considered satisfactory enough and the Bohm/gyro-Bohm model (that was specifically developed for simulations of JET plasmas) is adopted for predictive simulations in the following. The first example, shown in Fig.13, concerns the impact of enhanced NBI power (32 MW instead of 14 MW) on the H-mode scenario of Pulse No: 73344. Despite the high density, which tends to equilibrate the electron and ion temperatures, the increased NBI power causes an increased difference in the temperatures of both electron and ion channels (Fig.13), owing to the fact that in this parameter range the NBI power is mainly deposited on the ions: the electron/ion power deposition ratio Pe/Pi is in this case of the order of 0.6. It is a main function envisaged for the ECRH system to provide central electron heating, in order to equilibrate the two channels, thus making the JET Hmode more similar to that projected for ITER. In order to provide pure heating in the core region, a combination of co- and counter-injected EC wave beams is adopted (5MW per beam, toroidal injection angles

±20°). Since at the relatively low magnetic field used in this simulation ($B \approx 2.67$) a significant fraction ( ≈ 50%) of the wave power launched in the Xmode would have been absorbed at the third harmonic in a broad plasma region ($\rho = 0.2 - 0.6$), the O-mode is used, which provides still good but more central power absorption, as shown in Fig.14. The result is an electron temperature which is slightly higher than the ion temperature, as shown in Fig.15. Note that, in this case, $P_e/P_i \sim 1.13$ is obtained. It is possible therefore to conclude that an ECRH power of the order of 10MW is needed in JET, at high power and high density, in order to attain a $T_i/T_e$ ratio similar to that of an ITER H-mode. A scan of the NBI power $0 < P_{NBI} < 32$MW would then allow to explore electron/ion power share conditions approaching those of ITER ($P_e/P_i \sim 2$).

The main application of EC waves to JET advanced scenarios is now considered. It consists in using off-axis ECCD to produce a significant change of the q profile, with a shear inversion that could reinforce the ITB (produced in these scenarios by the combination of strong rotation and weak shear) or control its dynamics. This gives at the same time more non-inductive and more bootstrap current, opening up the possibility of obtaining controlled fully non-inductive discharges in JET at high power and moderately high density. In the following simulations, the predictive run of JET Pulse No: 77895 is used as a target for injecting 10MW of EC power, in the X-mode polarisation, with a toroidal angle of 25° (in order to optimise the CD efficiency) and poloidal angles appropriately chosen in order to modify the q profile at $\rho \sim 0.5$ or 0.6. A large peak is produced in the current density profile, corresponding to a driven current ~ 200kA. The location of the peak can be controlled by tilting the poloidal angles, e.g., a 6° change causes the peak to move to $\rho \sim 0.6$. The effect of this ECCD current on the q profile and on the temperature profiles is shown in Fig.16. It appears that the ITB, in particular the ion one, is strongly reinforced. On the other hand, additional electron heating would be needed inside the ITB in order to enhance the electron temperature too. Owing to the additional non-inductive current provided by ECCD and to the additional bootstrap current associated with the ITB steepening, these simulations correspond to a fully (or close to fully for EC deposition at $\rho \sim 0.5$) non-inductive discharge [26].

A second example is the application of ECCD at $\rho \approx 0.3-0.4$, with the aim of flattening the q profile in order to assist and control the formation of a hybrid-like scenario. This is similar to the EC-assisted hybrid scenario for ITER discussed in [6]. The main parameters of this CRONOS simulation are those of Pulse No: 77895 77895, but with a higher electron density ($n_{e0} = 7.2\times10^{19}$ $m^{-3}$), slightly higher magnetic field ($B_0 = 2.9$T) and slightly different heating mix ($P_{NBI} = 20$MW, $P_{IC} = 4$MW, $P_{LH} = 0$). The various current density profiles and the q profile are shown in Fig.17 (dashed curves without EC waves, solid curves with EC waves). Without EC waves, the q profile drops in time to $q_0 \sim 1$. Conversely, 8MW of ECCD applied for $t > 4$ s are sufficient to flatten the q profile inside $\rho \approx 0.45$, and obtain a scenario with $\beta_N = 3$, bootstrap fraction $f_{bs} \approx 60$ % and non-inductive fraction $f_{ni} \approx 80$ %. Since the EC power used was only 8MW, a substantial margin of ECRH power would still be available for operation at higher current and/or density, or for q profile flattening in a broader region.

In conclusion, scenarios at higher heating power and with ECRH/ECCD have been simulated. It is found that a wave power of the order of 10MW, absorbed in the central plasma region, is adequate in order to equilibrate electron and ion temperatures in the H-mode scenario. For advanced scenarios, 10MW of off-axis ECCD is marginally adequate to significantly modify the q profile. These calculations also indicate that fully non-inductive discharges at high power and density can be achieved. Nevertheless, a full inversion of the q profile inside the radius of ECCD absorption does not seem possible, owing to the dominant contribution of the current driven by the NBI power [26]. Note that with the use of LHCD in the current ramp-up phase an ITB can be triggered, however it is lost after a few seconds. The use of off-axis ECCD allows to sustain this ITB for times of the order of the full JET flat-top pulse at high power (~ 20s). Finally, it should be mentioned that these calculations do not include possible synergy effects between ECCD and LHCD, that have been observed experimentally on Tore Supra [27]. They can be quantified by a synergy factor defined as $Fsyn = (I_{LH+EC}-I_{LH})/I_{EC}$, where $I_{LH+EC}$, $I_{LH}$ and $I_{EC}$, respectively, are the currents driven by the two waves together and by the LH and the EC wave separately. The same Fokker-Planck code [28] used for the successful comparison with Tore Supra data has been used to estimate the synergy effect on JET, for the parameters of the advanced scenario. In this case, a synergy factor $F_{syn} \approx 1.5$ is computed. This enhancement would have a significant impact on the use of ECCD as a tool for q profile tailoring. However, it would require optimum overlap of the two interaction regions and good penetration of the LH waves, which is not always guaranteed in high density JET plasmas. For this reason, the conservative assumption of no synergy effect has been used in this study.

## 4. SYSTEM COMPONENTS AND CONCEPTUAL DESIGN

### *4.1 GYROTRONS*

The availability of powerful gyrotrons is an obvious prerequisite for making an ECRH system of this size a success. The requirement of 10 MW EC power absorbed in the plasma, leads to the definition of an installed power of 12 MW, in order to cope with transmission power losses and with the possible unavailability of one gyrotron (a likely event in a large heating system of this type). The production of up to 12 gyrotrons of 1MW unit power is likely to be on the critical path of the construction of an ECRH system for JET and hence much attention was paid to the state of gyrotron development. Various gyrotron frequencies have been considered, not only for the physics studies, but also from the point of view of their state of development. In order to limit the complexity of the system, a unit power of 1MW and a pulse length of at least 20s (corresponding to the typical limitation for high power discharges in JET) have been assumed as required. In particular, industrial availability of adequate power sources produced by the Russian partners has been investigated. The Russian company GYCOM can provide gyrotrons satisfying the requirements for both frequency options considered in the physics studies [29]. Every year from 3 to 5 gyrotrons are manufactured and tested by cooperation of the Institute for Applied Physics (Nizhny Novgorod), GYCOM and the Kurchatov Institute.

A 170GHz gyrotron with the required specifications already exists: it is the tube developed for ITER, which has already attained performances exceeding 1 MW, 570s pulse duration [30]. Efficiency, defined as ratio of power in the paraxial part of the output wave beam to power of the main power supply was 53-55%. A double-frequency 113-150GHz gyrotron would require a modest development with respect to the existing 105-140GHz, 10s tubes developed for Asdex Upgrade. The present industrial production capability of GYCOM is of 5 tubes per year. The delivery of 12 gyrotrons for JET would be favourably phased with respect to that of 8 gyrotrons for ITER. Therefore, the production of 12 gyrotrons in 4 years appears a reasonably achievable target, with minimum risk.

### *4.2 GENERAL LAYOUT, TRANSMISSION LINES, WINDOWS*

Finding an adequate port and location for the EC system in the present JET environment is not easy. Four port options have been identified: octants 1, 2, 5, or 6. Octant 6 would require relocation of a large number of diagnostics, while only one or two diagnostics would have to be moved in the case of octants 1 or 5. The diagnostics in octants 1 and 5 are however rather bulky and finding a suitable location for these in other octants poses significant problems. I additions octants 1 and 5 are used for access inside the tokamak during maintenance and hence an ECRH launcher placed in these octants would have to be removed every time invessel maintenance was required. Following these considerations octant 2 has been chosen as the reference solution. This requires the removal of the. ITER-like ICRH antenna, which is presently not functioning from octant 2.

Four different locations for the EC system (gyrotrons with auxiliaries and power supplies) have been identified, most of them requiring the construction of new buildings [31]. A floor area requirement of approximately 480 m2 has been estimated, in 3 storeys, with cooling plant on the ground floor, gyrotrons on the 1st floor and body power supplies and other auxiliaries on the 2nd floor. To allow the maximum spacing between gyrotrons it is proposed to distribute the equipment in a 4×3 pattern. It is proposed that the power supply equipment associated with a gyrotron is situated directly above the enclosure of the gyrotron in question. With such a layout, isolating individual gyrotrons electrically without shutting down the complete plant, becomes easier to handle.

The basic question of choice between quasi-optical and waveguide transmission has been addressed. Although in the considered frequency range the two options could be equivalent for a new machine environment, the quasi-optical approach seems difficult to implement in the very busy environment of JET while complying with the safety requirements connected with tritium operation. The ITER-relevant evacuated waveguide solution is considered preferable from the technical, safety and cost points of view and has been used as a reference solution for the JET ECRH system. It consists of evacuated corrugated aluminium waveguides with an internal diameter of 63.5 mm, connecting the gyrotrons to the launcher with mechanical continuity. The 12 lines can be allocated in a bundle of 1×1.2m with 0.3m of inter-axis separation in the seciton from the gyrotron building to the torus hall wall. The transmission efficiency is very high (~95%). A list of necessary components has been defined on the basis of the experience on similar systems:

- Aluminium corrugated waveguide (63.5mm i.d., HE1,1 low loss mode).
- 90º mitre bends, with plane mirrors; they are responsible for most of the losses, mainly due to the diffraction and mode conversion.
- Beam Switch to direct the power into the load. It can be integrated in the Matching Optics Unit to simplify the layout and the distribution of components.
- Polarizer made of 2 mitre bends equipped with rotating corrugated surfaces (depth $\lambda/4$ and $\lambda/8$) remotely controlled in real time.
- Power monitor, i.e. a single mitre bend with detectors in both directions, located as close as possible to the launcher.
- Sliding joints (bellows) to compensate for length variation due to mechanical stress.
- DC break at the Torus Hall entrance.
- Gate valves: one standard before the vessel and one fast at the Torus Hall entrance for Tritium containment.
- Pumping unit: two groups to evacuate waveguides to 10-5mBar through Pumping Tees.
- Load: 1MW/20s (cw equivalent) for every gyrotron.

The principal components exist and are routinely produced and tested at MW level. Having selected the evacuated waveguide transmission solution, the best location for the Gyrotron plant, allowing the simplest transmission line routing to the launcher, was identified [32]. With this choice the plant would be in a new building and the resulting transmission line would be ~75 m long, with only 6 bends and expected attenuation of 4.1 %. A preliminary design of the transmission lines in the torus hall is shown in Fig. 18. To avoid neutron streaming from JET out of the Torus Hall, in particular during tritium operation, appropriate neutron shielding will be required close to the waveguide penetrations through the torus hall wall.

Vacuum windows in the transmission lines are required to segregate the tokamak vacuum from the transmsission line vacuum thereby preventing the migration of tiritium into the transmission line. Synthetic diamond windows are the only viable solutions, considering the power / pulse length combination. Since 170 GHz is chosen, the same windows used for the ITER ECRH system could be employed, with substantial synergy with the ITER ECRH system development. The use of two windows per line (for tritium segregation) was initially considered [32]: in this case, two separate windows (one at the entrance of the Torus Hall and the other at the vacuum vessel) are preferable to a double window, from the safety point of view. However, the time necessary to produce such a large number of windows (24) is presently difficult to determine and could be a source of delay. The single window solution has also been investigated and a thorough assessment has concluded that installing a single diamond window in each waveguide near the torus is sufficient for tritium containment. The single window solutions has therefore been chosen as the reference option. The behaviour and lifetime of these windows is a significant element of risk, but also a contribution of risk reduction for the ITER ECRH system. In order to reduce the risk of contaminating the line with tritium in the case of window damage, a standard valve, permitting the window to be removed

without breaking the JET vacuum, is required. Another (fast) valve situated near the torus hall wall will isolate the torus hall from the rest of the world when the line in the torus hall is disconnected, as will be required for certain JET shutdown activities. This second valve will also serve to rapidly isolate the torus hall transmission line from the transmission line outside the torus hall in case of window breakage and risk of tritium migration into the transmission line.

Particular care must be used in the definition of a window fault test strategy. A possible arrangement is shown in Fig.19. Systematic checks should be performed with Nitrogen injection in the section between the diamond window and the standard gate valve. If the window fails during the operation, this is likely to be associated with the detection of an electric arc at the window or an anomalous pressure increase in the torus hall waveguide section. The detection of either of theses fault conditions should lead to the closure of both the standard valve near the tokamak and the fast valve near the torus hall wall, isolating the line from the vessel. After the closure of the valves operation can continue with the other transmission lines. In the case of window failure during operation with tritium, the tritium detector installed on the pumping unit close to the window will automatically cause the interlock system to close the fast valve (and the slow valve). The fast valve has to react sufficiently quickly to prevent tritium to migrate along the transmission line from the window into the vawguide section outside the torus hall. Finally, a preliminary safety analysis has been performed. It has been determined that the ECRH system would be classified as Tritium Class 2, i.e., 'a system with a low potential for routine/accidental release and exposure of personnel or systems necessary to prevent/limit release or exposure for Class 1 systems under fault conditions'.

### *4.3 LAUNCHER*

Various options for a launcher design have been analysed, with the following requirements: plug-in launcher fitting in an equatorial port fed by 12 waveguides; toroidally and poloidally steerable actively cooled mirrors, use of the ITER steering mechanism [33] for at least one of the two movements. The available space in the port and the port shape suggested considering a two-module system, i.e., one set of mirrors in the upper part of the port and one in the lower part, each launching 6 beams. On this basis, three main options and various sub-options have been considered [34], all of them using the ITER steering mechanism for the poloidal movement (which should be controlled in real time) and a simpler solution for the toroidal movement, allowing toroidal steering on a shot-to-shot basis. Figure 20 shows a sketch of the option selected for conceptual antenna design with the ITER steering mechanism located at the back of the port where more space is available. This is a top view, where only the upper module of the antenna is shown, the lower module being the mirror image of the upper one. One module is made of the following components:

- 6 tapered waveguide terminations,
- 6 focusing mirrors with ellipsoidal surface,
- one ITER steering mechanism providing the poloidal steering of a flat mirror,
- one toroidal steering mechanism moving one flat mirror,

– one fixed side mirror shared by the two modules, used for counter-CD.

The antenna relies on the propagation of Gaussian beams emitted by waveguide terminations (tapers) located at the port back plate. From the waveguides the beams diverge until they encounter fixed focusing mirrors which direct the beams, in groups of 6, onto a plane poloidal steering mirror mounted on the ITER steering mechanism. Rotating this mirror around a horizontal axis allows control of the poloidal injection angle. After the poloidal steering mirror, the beams encounter the toroidal steering mirror; a large vertical mirror that can be rotated around a vertical axis for toroidal injection angle control. For co-current drive the beams are injected directly from the toroidal steering mirror. By rotating the toroidal steering mirror beyond the point corresponding to the maximum positive toroidal injection angle the beams will be reflected by the final vertical mirror allowing counter-current injection.

This option allows full coverage of the poloidal and toroidal angle range defined by the beam-tracing studies. Moreover, it implements the ITER steering mechanism without any modification. This conceptual design has been implemented in the GRASP Physics Optics tool [35] and the beams propagation in the optical system has been studied and optimised. The waveguides will be terminated by specifically designed tapers in order to improve the purity of the emitted Gaussian beams [36]. These tapers are implemented for the following purposes:

– Shift the beam waist into the taper by a distance Dz in order to increase the effective optical propagation distance din between the beam waist and the focusing mirror. This reduces the physical length of the optical system, i.e., makes the antenna more compact, avoiding the use of a costly port extension on the back.
– Decrease the stray radiation by improving the coupling efficiency between the HE11 mode propagating in the waveguide and the Gaussian beam propagating in the antenna. This coupling efficiency which is 98% with an open ended standard waveguide can be improved to almost 100% by the appropriate taper design.
– Change the waist radius $w_0$ of the beam, i.e., improve the focusing

With an optimised taper design, $\Delta z = 911$mm and $w_0 = 20.43$mm, a beam transverse dimension in the centre of the plasma of the order of 40mm can be achieved, to be compared with 65mm if no tapers were used. An extensive analysis of the resistive losses and of the thermal loads in the launcher has been performed. Several options have been considered for the mirror material and cooling techniques:

– stainless-steel mirrors and water-cooled copper surface, with cooling pipes close to the reflecting surface.
– uncooled massive (thickness ≥40mm) copper (or CuCrZr) or TZM alloy (Mo99/Ti 0.5/Zr 0.1) mirrors with copper or gold-coated surfaces.
– uncooled graphite (thickness ≥40mm) mirrors, gold-coated or copper-coated.

It is found that that the uncooled options do not comply with the expected pulse rate of JET. A possible way to avoid thermal runaway in this case is to use He gas cooling between shots in order to recover the original temperature. Printed Circuit Heat Exchanger (PCHE) technology has also been suggested for the manufacturing of the bulk substrate for water-cooled mirrors. Such a technique provides efficient heat exchange by chemical etching of small channels in thin plates of the bulk material (stainless steel 316 or other alloys suitable for temperatures in excess of 800–900°). The plates are joined together to form the complete channel matrix by diffusion bonding. All the options here mentioned need further analysis including thermomechanical calculations.

For toroidal steering of the beams, two mirrors with a typical size of 40×40cm$^2$ and a steering range of 25° will be used. These mirrors will be actuated by a push-pull rod. The mirrors consist of a cooled support structure and a bonded (brazing / Hot Isostatic Pressing) reflection surface. To fix the mirror precisely, two fasteners are welded to the plug structure. Two customized shims provide compensation of manufacturing tolerances and are connected to pivot joints. The joints consist in principle of a bolted flange and two flexure pivots to enable frictionless and backlash-free rotation of the mirror. The push-pull rods are connected to the movable mirror by a hinged bracket. It is mounted parallel to the poloidal position of one of the flexure pivots in order to avoid moments perpendicular to the rotation axis of the mirror.

A comprehensive picture of the antenna design is shown in Fig.21, where only the focusing and steerable mirrors of the upper module are shown for clarity. Note the pentagon arrangement of the tapers at the port flange, the focusing mirrors, the steerable mirrors with their mechanisms and the large counter-CD mirror. All these mirrors are mounted inside a plug that matches the shape of the JET equatorial port, therefore the ensemble constitutes a plug-in unit, as required for easy maintenance.

A stress analysis has been performed on a slightly simplified geometrical model: a cylindrical section on the backside, a rectangular/trapezoidal section on the plasma side and a transition section in the middle. Conservative assumptions on the electro-magnetic disruption forces have been adopted, close to lowest limit of the yield strength of Inconel 625 (400MPa). Finite element computations have been carried on using the same codes and methods that are being used for the ITER Upper Launcher design [37]. An example of the deformations of the plug structure due to electromagnetic forces associated with disruptions is shown in Fig.22.

### *4.4 POWER SUPPLIES.*

The 170GHz GYCOM gyrotrons require a main power supply rated at –65kV, 50A and a body power supply rated at 30kV, 50mA. The possibility of using an existing NBI power supply, manufactured by Siemens 27 years ago and no longer in use at JET, has been analysed. It has been found that half of this system can be used with minor modifications while the other half requires major refurbishment. The modification of both halves nevertheless seems both technically and economically attractive. An approach based on the use of the refurbished NBI powers supplies (Type 1) to supply 8 gyrotrons

and 4 new power supplies (Type 2) for the remaining 4 gyrotrons has been developed [38].

The Type 1 Power Supply consists of a rectifier transformer and a tetrode tube regulator connected in series to the transformer DC - output: the old transformers are re-used here, with new star-point controllers. The tetrode regulator with its associated crowbar unit serves both for voltage regulation and for protection. The Type 2 power supplies consists of new solid-state technology power supply, either PSM (Pulse Step Modulation) or primary clocked switch mode. Corresponding requirements for the body voltage power supplies have also been determined. The use of a tetrode regulator in the type 1 power supplies has the significant advantage of allowing fast power modulation (15-20kHz), which is useful for NTM control, whereas PSM power supplies (the technology adopted for the ITER ECRH system) would be limited to 5kHz.

The risk assessment concerning the refurbishment and reconstruction of the tetrode regulator units has shown that the proposed design based on the use of tetrodes as series voltage regulators represents an acceptable level of risk provided all old electronics equipment is replaced. To further limit the risk, an alternative voltage regulation scheme has been evaluated. This scheme would replace the tetrodes in the reference design with solid state devices. The availability of this solution in case of problems with continued tetrode delivery represents a significant risk reduction and no major changes to the rest of the plant are required in order to exchange tetrodes with solid state solutions. While this alternative solution may prove attractive in the future, it is considered that the use of tetrode regulators remains the solution promising the widest operating range and lowest level of risk, cost and effort. The cost could increase fractionally in the case of a required tetrode replacement. If neither tetrode tube supplier (TED and CPI) confirms the availability of tetrodes until 2020, then one of the solid state based solutions would be required for all 12 gyrotrons. At present the PSM based solution would probably be the preferred choice in this case for various reasons e.g. cost, ITER relevance, reliability, and the fact that it is a proven and tested solution.

### *4.5 AUXILIARIES, CONTROL SYSTEM, DIAGNOSTICS*

A significant amount of auxiliary equipment and services are required to make the ECRH plant operational: cooling water, superconducting magnets for the gyrotrons, auxiliary power supplies (for the superconducting magnets, filaments, collector sweeping magnets, ion pumps), vacuum pumps and gauges, compressed air, motors for moving polarisers, mirrors and switches, arc detection systems, microwave measurement systems, etc. The requirements for all these auxiliary systems have been analysed [39], using the GYCOM gyrotron specifications. A significant cost will be associated with these auxiliaries, in particular with the superconducting magnets, which produce the magnetic field in the gyrotrons (of the order of 7T for a 170GHz tube). These magnets have to be cooled to temperatures of the order of a few Kelvin. Traditionally, this cooling is done using liquid helium and liquid nitrogen. The magnet cryostat in such a system typically has to be filled with liquid helium at least once but more likely twice a week. The filling can be carried out manually but this seems unrealistic for a plant with 12 gyrotrons. More realistically, an automatic

cryo distribution system could be used and the cryostats could be filled regularly outside operation hours. 1200 litres of liquid helium and 1200 litres of liquid nitrogen per week would typically be needed, which is beyond the capability of the present JET cryogenic plant. An additional He liquefier dedicated to the ECRH system would therefore be required. Using traditional cryo magnets, the cost and availability of helium is another important issue which has to be considered. With the proliferation of Magnetic Resonance Imaging scanners in hospitals around the world, using powerful cryomagnets, an alternative to magnets cooled by external cryo liquids, has become economically competitive. The so-called 'cryogen free' systems are 'stand alone' systems including magnets, refrigerators etc. They cost more than ordinary cryo magnets and they consume a fair amount of power (10-15 kW each continuously), but estimates performed for the DIII-D gyrotron system have concluded that changing to cryogen free systems is preferable considering the present cost of helium and electricity. In addition to the cost saving associated with the use of cryogen free magnets a significant improvement in operational convenience should also be achieved. Based on these considerations and noting that the ITER ECRH system will use cryogen free systems it is proposed that the JET ECRH system should also use cryogen free magnets..

The JET ECRH project would yield a good opportunity to design a control system that adopts and tests a number of ITER-CODAC (Control, Data Access and Communication) standards, possibly in close connection with the ITER-CODAC group. This includes central timing, storage, interlocks, cross-subsystem control etc. It is therefore proposed that the Control and Data Acquisition system should be based on the ITER-CODAC/I&C design. Accordingly 'slow' instrumentation and control should use the Siemens S7 PLC (Programmable Logic Control) range while using a model of the ITER CODAC Plant System Host (PSH) computer for communications with the PLC. Above this host level, standard JET CODAS 'black-box' software should be used. For the safety systems, CISS (Central Interlock and Safety System) and PSACS (Personnel Safety and Access Control System), standard JET procedures will be followed.

A number of diagnostics, in particular microwave based ones, will require adequate protection from stray radiation produced by the gyrotrons. Stray radiation caused by ECRH power is assumed to be a few mW in normal operation, and may rise by a factor of 100 to 1000 under fault conditions. For the latter case, if components can handle 10dBm (10mW) a 40dB rejection at 170GHz is needed. A narrow frequency width (~1GHz) is assumed for the 170 GHz source, to take into account any frequency jitter - particularly during switching.

Some of the potential impacts and interferences are listed below:

1. Testing of the gyrotrons into the empty vacuum vessel. In order to bring the system into operation it may be necessary to inject short ECRH pulses (less than 100 ms) into the JET vacuum vessel in the absence of plasma. This could be used for antenna commissioning, or in case of plasma startup experiments assisted by ECRH. For this particular case the following issues need to be considered:

- Personnel access to diagnostic areas coupled to the vacuum vessel or even directly to the torus hall has to be restricted/ prohibited.
- Shutters in all waveguides and quasi-optical connections connected to plant or back to populated areas have to be closed. If such shutters does not exist at present they have to be installed.
- Covers have to be installed on unused windows on the vacuum vessel to prevent stray radiation escaping from the vacuum vessel.
- The risk of damage to windows or other in-vessel components due to absorbed power has to be assessed.
- The pulse length and repetition rate of gyrotrons for this type of operation has to be limited. A fail safe protection system preventing the injection of longer/more frequent pulses have to be implemented.
- The fairly broad mode spectrum of gyrotron, in particularly during switch on or power modulation, has to be considered.

2. Protection of diagnostics during abnormal events occurring in ECRH operation, such as disruptions or low power absorption (because of unsuitable plasma parameters) leading to shine through or strong reflections. For these cases the pulses should be terminated prematurely and a fast gyrotron interlock system should be implemented to provide failsafe protective termination for a range of gyrotron and plasma fault conditions. In this case:
    - some changes to the JET 'Plant Enable Window System' (PEWS), that monitors plasma parameters against set limits during a pulse, and the 'Pulse Termination Network' (PTN) interlocks will have to be implemented.
    - fast PIN diodes can be included for some sensitive waveguide systems
    - an array of 'sniffer' probes detecting stray 170 GHz radiations should be designed and implemented to detect high reflected power and to drive interlocks.

3. Interference and limitations to diagnostic operation during normal ECRH operation where small levels of non absorbed power might have an effect on data produced by some systems.
    - Band stop, high or low pass filtering may be required in systems where the ECRH frequency or its harmonics are in the bandwidth of the detector used in a diagnostic. This includes all the microwave diagnostics.
    - Restrictions to operation may be necessary to protect in vessel components where the resonance or a harmonic may lead to breakdown and absorption in pumped interspaces or near in-vessel components such as:- Magnetics (top coils and divertor in particular)
        - Feedthroughs and windows
        - Soft X-ray in-vessel arrays, TAE antennas, bolometers
        - Resonant magnetic perturbation coils
        - Quartz microbalances
        - Scintillator probe head

4. Personnel safety issues. It is assumed that the stray radiation caused by the ECRH power can reach values ~100W under fault condition. As this stray radiation propagates in small waveguides (dimensions of few mm), the power density ($W/m^2$) is quite high. In these conditions 1W is high enough to cause burns. The recommended safe RF power density levels are orders of magnitude lower. Therefore waveguides should not suffer any radiation leakage at 170GHz. Interlocks should be installed, for both waveguides and to gain access to all the affected areas: either (a) the ECRH plant is in a safe state or (b) the diagnostics waveguides shutters are closed.

## CONCLUSIONS

The usefulness of an EC system for JET is definitely confirmed by the physics studies and no strong limitations for any of the functions envisaged have been found. However, the power of 10 MW should be considered as a minimum, and some limitations in the magnetic field values at which the system can be used appear unavoidable, in particular for a single frequency system. The chosen frequency 170 GHz would maximise the synergies with the development of the ITER ECRH system. This choice takes into account physics requirements and properties, together with the availability of existing gyrotrons, the much simpler window concept (with respect to a double-frequency system) and the possibility of components and solutions being developed jointly with the ITER-IO and ITER Domestic Agencies teams.

In conclusion, an ECRH system for JET seems feasible, but it will be a complex project, with significant associated costs. From a technical point of view, the most critical issues concern the launcher design and the behaviour of new components such as the gyrotrons, the diamond windows and the mirror steering mechanism. However, these components are the same as for the ITER ECRH system, therefore their full scale test at JET would constitute a valuable risk reduction contribution to the ITER system. The total cost of the system is estimated ~ 55M€, assuming partial re-use of the existing power supplies. The manpower necessary for design, construction, tests, system commissioning on plasma and project management is estimated to 114 ppy. A preliminary planning is compatible with the delivery of 10MW ECRH power in the plasma in approximately 5 years, provided adequate funding and highly qualified manpower are available.

## ACKNOWLEDGEMENTS

This work was supported by EURATOM and carried out within the framework of the European Fusion Development Agreement. The views and opinions expressed herein do not necessarily reflect those of the European Commission. This work has substantially profited from V. Erckmann's invaluable experience, knowledge and wisdom. Help, encouragement and advice by C. Challis, L. Horton, E. Joffrin, F. Rimini and G. Sips are gratefully acknowledged.

**REFERENCES**


[1]. F. ROMANELLI, Fusion Science Technology **53** (2008) 1217.

[2]. J. PAMELA et al., Journal of Nuclear Materials **363-365** (2007) 1.

[3]. M. SHIMADA et al., Nuclear Fusion **47** (2007) S1.

[4]. C. GORMEZANO et al., Nuclear Fusion **47** (2007) S285.

[5]. C.E. KESSEL et al., Nuclear Fusion **47** (2007) 1274.

[6]. J. CITRIN et al., Nuclear Fusion **50** (2010) 115007.

[7]. A.G.A. VERHOEVEN et al., Nuclear Fusion **43** (2003) 1477.

[8]. M.A. HENDERSON et al., Nuclear Fusion **48** (2008) 054013.

[9]. D. FARINA, Fusion Science Technology **52** (2007) 154.

[10]. J.F. ARTAUD et al., Nuclear Fusion **50** (2010) 043001.

[11]. D. FARINA, L. FIGINI, Nuclear Fusion **50** (2010) 095007.

[12]. S. NOWAK, in Proceed. of the 16th Joint Workshop on ECE and ECRH (World Scientific, Singapore, 2010).

[13]. E. LAZZARO, S. NOWAK, Plasma Physics and Controlled Fusion **51** (2009) 035005

[14]. F.L. WAELBROECK and R. FITZPATRICK, Physics Review Letters **78** (1997) 1703

[15]. C. ANGIONI et al., Nuclear Fusion **43** (2003) 455

[16]. D.A. KISLOV for the T-10 team, Nuclear Fusion **47** (2007) S590

[17]. H. ZOHM et al., Nuclear Fusion **47** (2007) 228

[18]. M. LENNHOLM et al., Physics Review Letters **102** (2009) 115004

[19]. M. LENNHOLM et al., Fusion Science Technology **55** (2009) 45

[20]. G.V. PEREVERZEV, P.N. YUSHMANOV, ASTRA-Automated System for Transport Analysis, IPP 5/98, February 2002.

[21]. F. PORCELLI et al., Plasma Physics and Controlled Fusion **38** (1996) 2163.

[22]. O. SAUTER et al., Physics of Plasmas **6** (1999) 2834

[23]. C. ANGIONI et al., Plasma Physics and Controlled Fusion **44** (2002) 205

[24]. G. CENACCHI, A. TARONI, JETTO: a free boundary plasma transport code, ENEA, RT/TIB/5/ 1988.

[25]. M. ERBA et al., Plasma Physics and Controlled Fusion **39** (1997) 261.

[26]. J. GARCIA et al., Nuclear Fusion, submitted for publication (2010).

[27]. G. GIRUZZI et al., Physics Review Letters **93** (2004) 255002.

[28]. G. GIRUZZI, Plasma Physics and Controlled Fusion **35** (1993) A123.

[29]. G.G. DENISOV, A.G. LITVAK et al., Nuclear Fusion **48** (2008) 054007.

[30]. A.G. LITVAK et al., in 23rd IAEA Fusion Energy Conference, FTP/1-2Ra (Daejon, Oct. 10-16, 2010).

[31]. M. LENNHOLM et al., 26th Symposium on Fusion Technology (2010), Fusion Engineering and Design, to be published.

[32]. S. GARAVAGLIA et al., in Proceed. of the 16th Joint Workshop on ECE and ECRH (World Scientific, Singapore, 2010).

[33]. R. CHAVAN et al., Fusion Engineering Design **82** (2007) 867.
[34]. C. SOZZI et al., in Proceed. of the 16th Joint Workshop on ECE and ECRH (World Scientific, Singapore, 2010).
[35]. K.Pontoppidan, GRASPÒ Tech. Description, TICRA, Denmark (2005).
[36]. B. Plaum et al., Workshop on RF Heating Technology of Fusion Plasmas 2010 (Como, September 13-15, 2010).
[37]. A. VACCARO et al., Fusion Engineering Design **84** Issues 7-11 (2009) 1896.
[38]. H. BRAUNE et al., in Proceed. of the 16th Joint Workshop on ECE and ECRH (World Scientific, Singapore, 2010).
[39]. M. LENNHOLM et al., in Proceed. of the 16th Joint Workshop on ECE and ECRH (World Scientific, Singapore, 2010).

| **Parameters** | **Pulse No: 73344 at t = 6.12s Standard H-mode** | **Pulse No: 77895 at t = 20.5s Advanced Scenario** |
|---|---|---|
| **$P_{nbi}$ [MW]** | 14.0 | 22.5 |
| **$P_{icrh}$ [MW]** | 1.5 | 6.6 |
| **$P_{lhcd}$ [MW]** | 0.0 | 2.3 |
| **$I_p$ [MA]/ $B_{tor}$ [T]** | 2.5/2.7 | 1.8/2.7 |
| **$q_{95}$** | 3.5 | 4.2 |
| **$R_{mag}$ [m] /a** | 3.0/0.9 | 3.2/0.9 |
| **$\kappa$ / $\delta$** | 1.74/0.41 | 1.75/0.41 |
| **$\beta_N$ / $\beta_p$** | 1.8/0.7 | 2.8/1.5 |
| **$l_i$** | 0.9 | 0.7 |
| **$n_l$ [$10^{19}m^{-3}$] / $n_l/n_G$** | 7.4/0.8 | 4.2/0.6 |
| **$n_{eo}$ / $n_{e\text{-}ped}$ [$10^{19}m^{-3}$]** | 8.3/6.6 | 5.8/3.6 |
| **$T_{eo}$ / $T_{e\text{-}ped}$ [keV]** | 4.2/1.5 | 8.2/2.5 |

*Table 1: Basic parameters of the two pulses selected for modelling.*

| Frequency (GHz) | Mode | Cutoff density ($m^{-3}$) |
|---|---|---|
| 113 | OM1 | $1.6\ 10^{20}$ |
| 150 | XM2 | $1.4\ 10^{20} \cos^2\phi$ |
| 170 | XM2 | $1.8\ 10^{20} \cos^2\phi$ |

*Table 2: Cutoff densities. OM1: O-mode, 1st harmonic. XM2: X-mode, 2nd harmonic. 90°−$\phi$ is the angle between the wave vector and the magnetic field.*

| q | $\psi$ | $\rho_t$ | $\rho_p$ | $\varepsilon$ | $r_s$ (m) | $L_q$ (m) | $L_p$ (m) | $\beta_p$ | $n_e$ ($10^{19}m^{-3}$) | $T_e$ (keV) | $I_p$, (MA) |
|---|---|---|---|---|---|---|---|---|---|---|---|
| 2/1 | 0.68 | 0.72 | 0.83 | 0.3 | 0.91 | 0.4 | 0.28 | 0.38 | 6.9 | 1.6 | 2 |
| 3/2 | 0.49 | 0.58 | 0.7 | 0.254 | 0.77 | 0.55 | 0.35 | 0.6 | 7.6 | 2.4 | 1.5 |

*Table 3: Main plasma parameters used in the Generalised Rutherford's equation for simulations of the NTM island evolution at q=2 and q=3/2.*

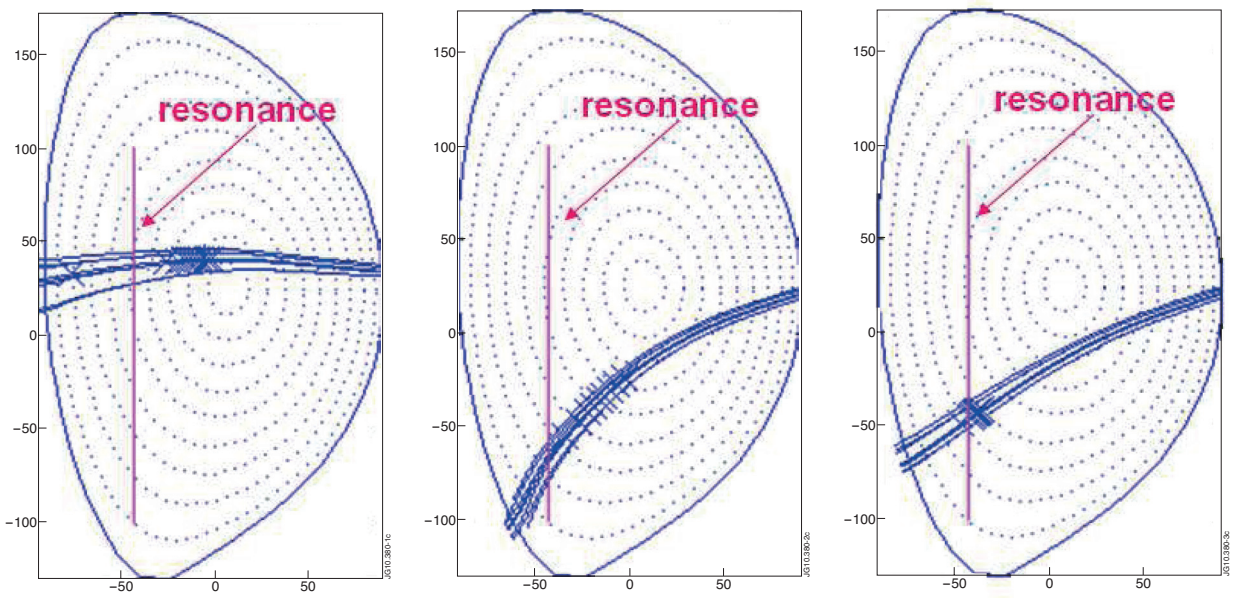


*Figure 1: Poloidal projections of EC wave trajectories in a JET plasma, computed by ray-tracing; each cross indicates the location of 10% wave absorption. Illustration of the use of toroidal injection angle (25°) and Doppler shift for core CD (left); of the use of poloidal injection angle for shift of CD to mid-radius (middle); of the use of a reduced toroidal angle (15°) to obtain more localised absorption for NTM control (right).*

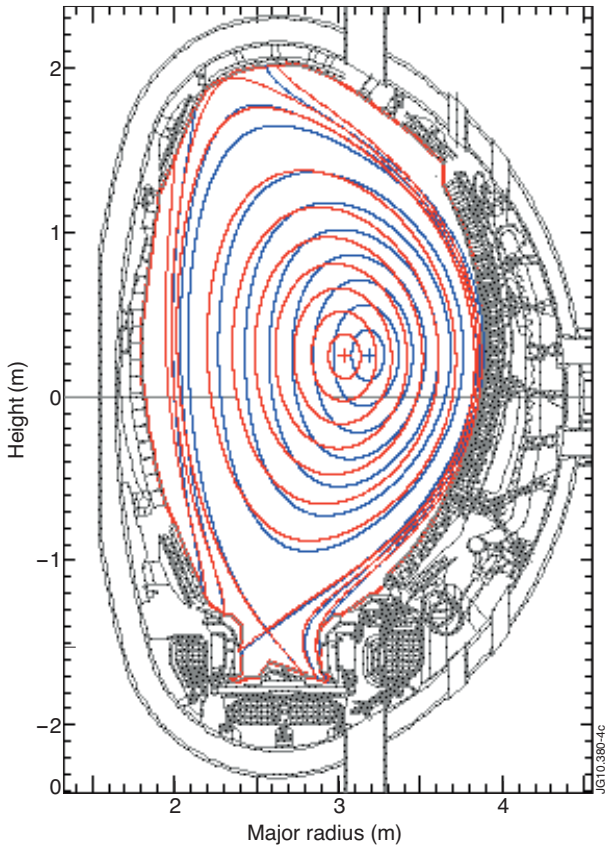


*Figure 2 : poloidal cross section showing the plasma magnetic equilibrium and iso-flux surfaces as computed from magnetic EFIT for Pulses No's: 73344 at t=20.5s (red) and 77895 at t=6 s (blue).*

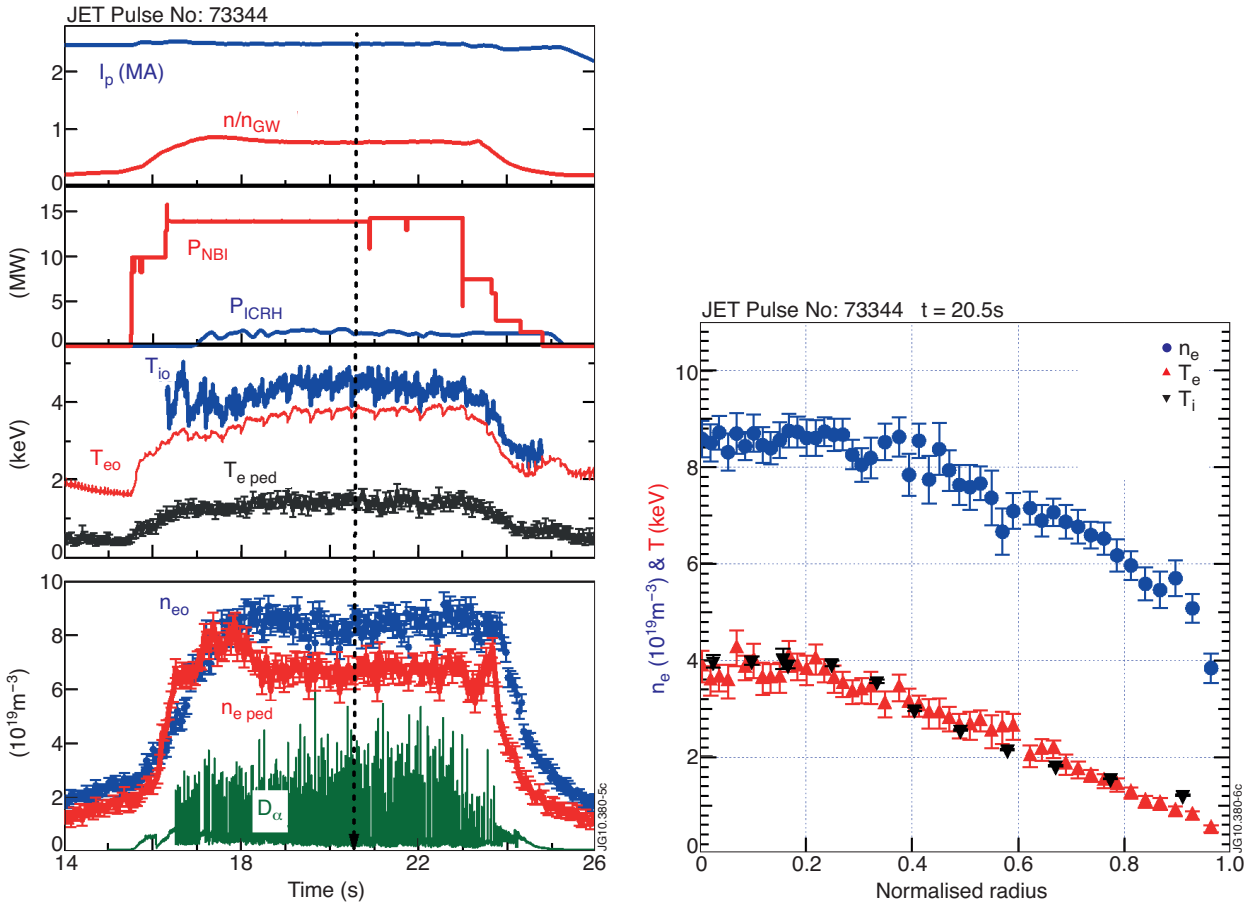


*Figure 3: Left: Time evolution of the main parameters for Pulse No's: 73344: Plasma current (Ip), line averaged density normalized to Greenwald density ($n/n_G$), NBI & ICRH powers ($P_{NBI}$, $P_{ICRH}$), core ion ($T_{io}$) and electron ($T_{eo}$) temperatures, electron temperature at the top of the pedestal ($T_{e\ ped}$), electron density at the centre ($n_{eo}$) and at the top of the pedestal ($n_{e\ ped}$), $D_\alpha$. Right: Electron density ($n_e$), electron and ion temperature ($T_e$, $T_i$) profiles measured with the high resolution Thomson scattering diagnostic (HRTS) and Charge Exchange spectroscopy at t=20.5s as indicated by the vertical arrow on the time traces. Note that t = 0 corresponds to t = 40s of the JET data base.*

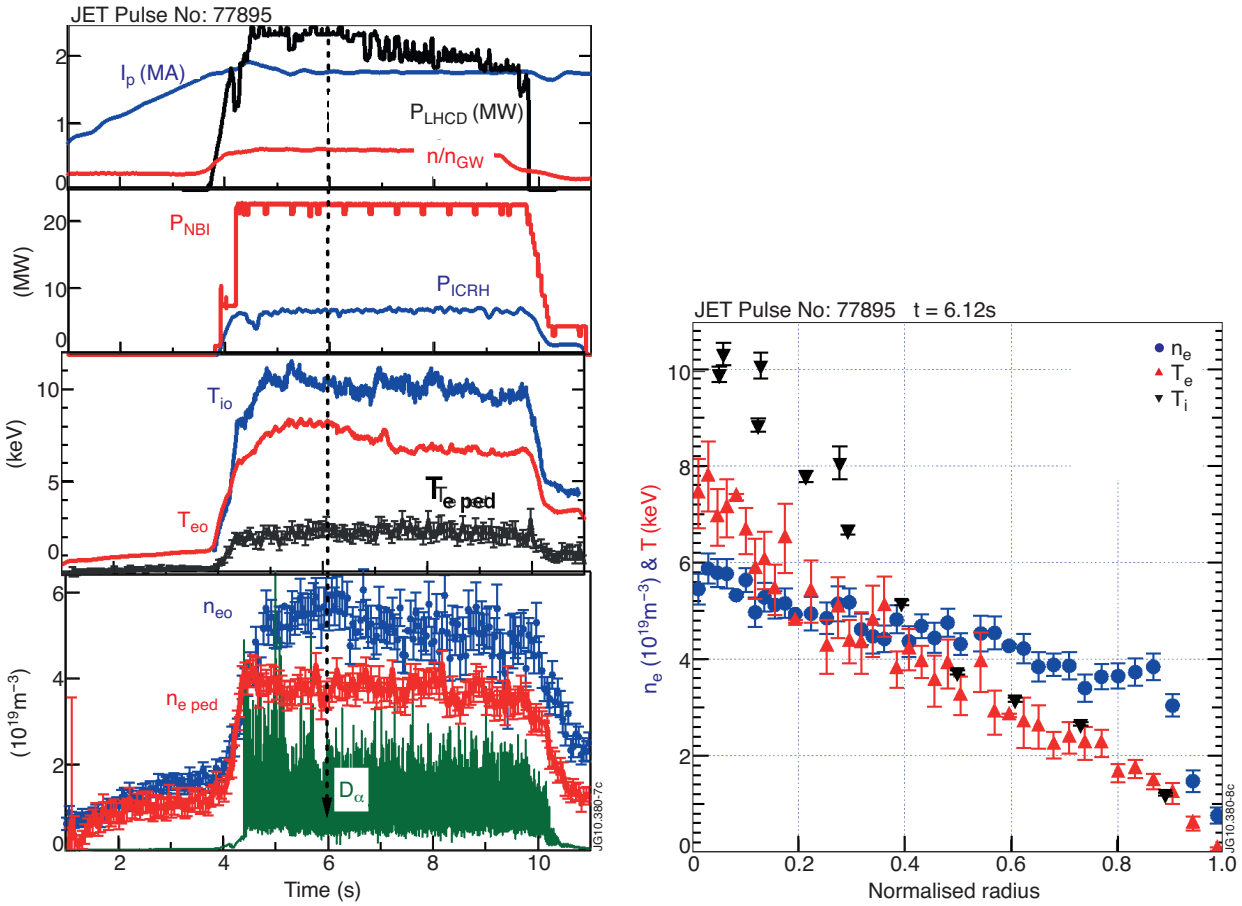


*Figure 4: Left: Time evolution of the main parameters for Pulse No: 77895: Plasma current ($I_p$), line averaged density normalized to Greenwald density ($n/n_G$), NBI, ICRH and LHCD powers ($P_{NBI}$, $P_{ICRH}$, $P_{LHCD}$), core ion ($T_{io}$) and electron ($T_{eo}$) temperature, electron temperature at the top of the pedestal (Te ped), electron density in the centre ($n_{eo}$) and at the top of the pedestal ($n_{e\,ped}$), $D_\alpha$. Right: Electron density ($n_e$), electron and ion temperature ($T_e$, $T_i$) profiles measured with the High Resolution Thomson Scattering diagnostic (HRTS) and Charge Exchange spectroscopy at t = 6.12s as indicated by the vertical arrow on the time traces.*

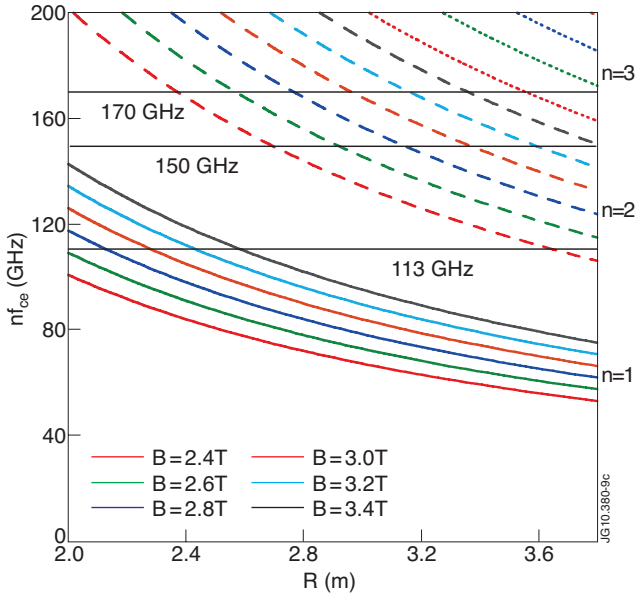


*Figure 5: Cyclotron harmonics as a function of the major radius for different values of the vacuum toroidal field in JET. Solid, dashed and dotted curves refer to first, second, and third harmonics, respectively. The three horizontal lines denote the frequency values, 113, 150, and 170GHz.*

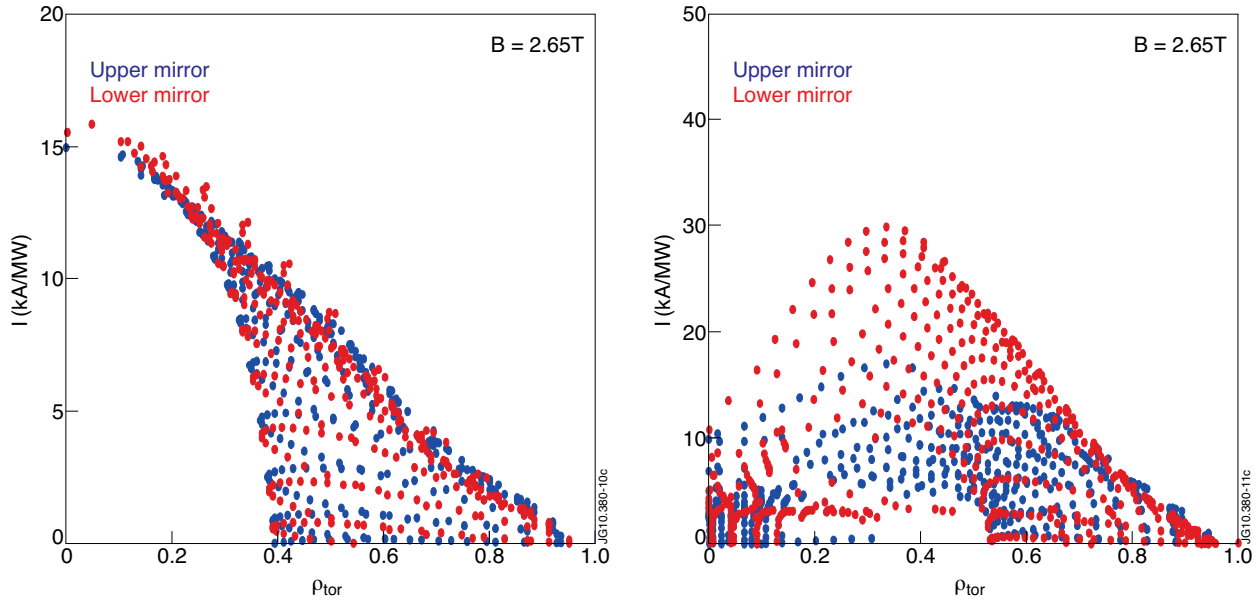


*Figure 6: EC driven current per MW of injected power versus radius for f = 170GHz, and Pulse No's: 73344 (left plot) and 77895 (right plot).*

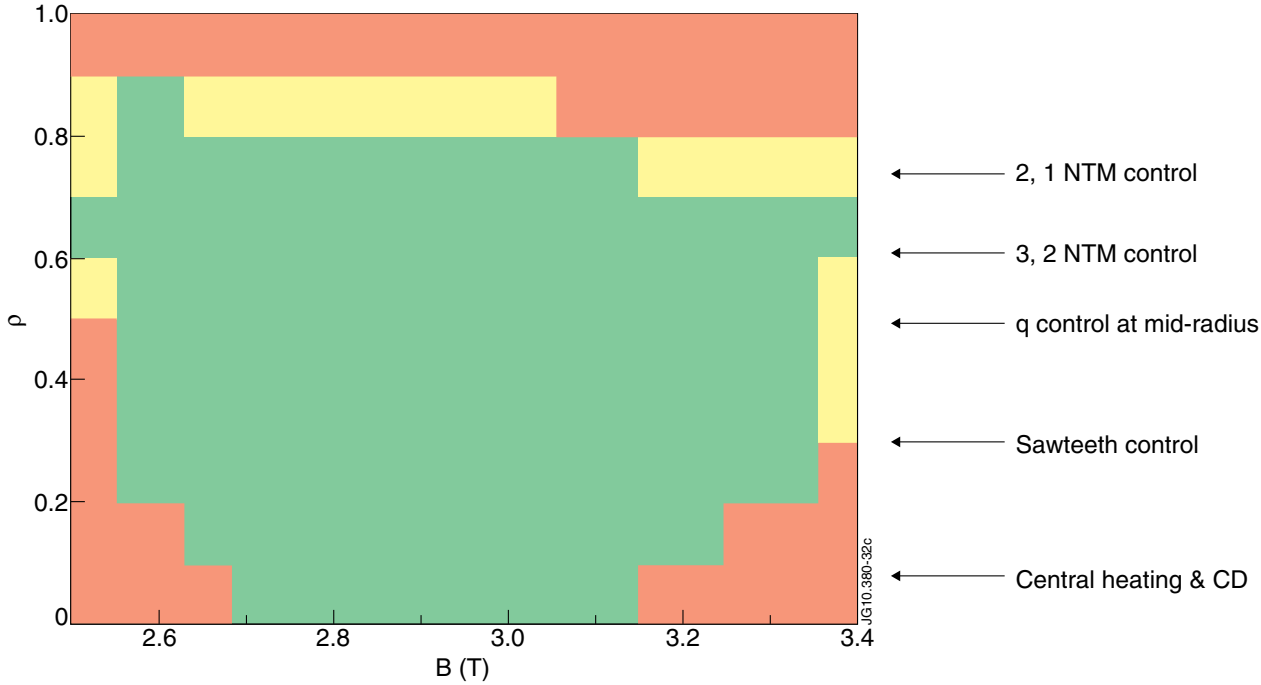


*Figure 7: Operation diagram for a JET ECRH system at 170GHz, computed for a reference H-mode scenario. Green means that the envisaged functions (listed on the right) are possible, red not possible, yellow marginally possible.*

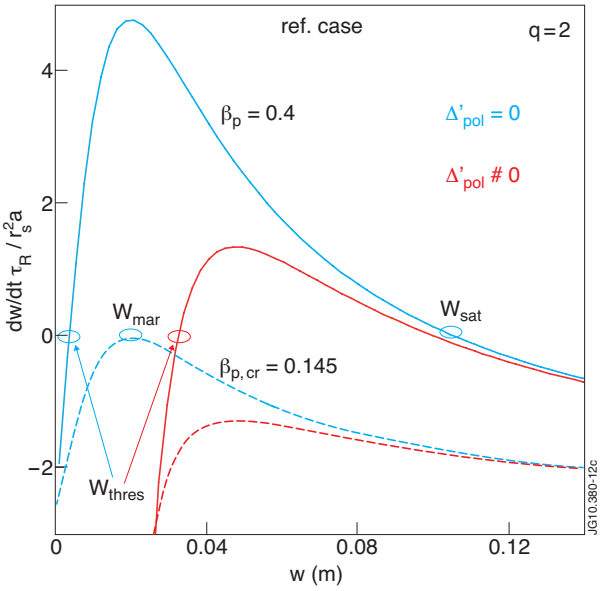


*Figure 8: Dimensionless growth rate of island evolution for parameters of reference shot (solid lines) for ion polarization term off (blue) and on (red). The marginal size of the island is obtained reducing the poloidal beta to the critical value 0.145 below which the mode is stable. The solid lines refer to bp =0.4, the dashed lines to the critical $\beta_{p,cr} = 0.145$.*

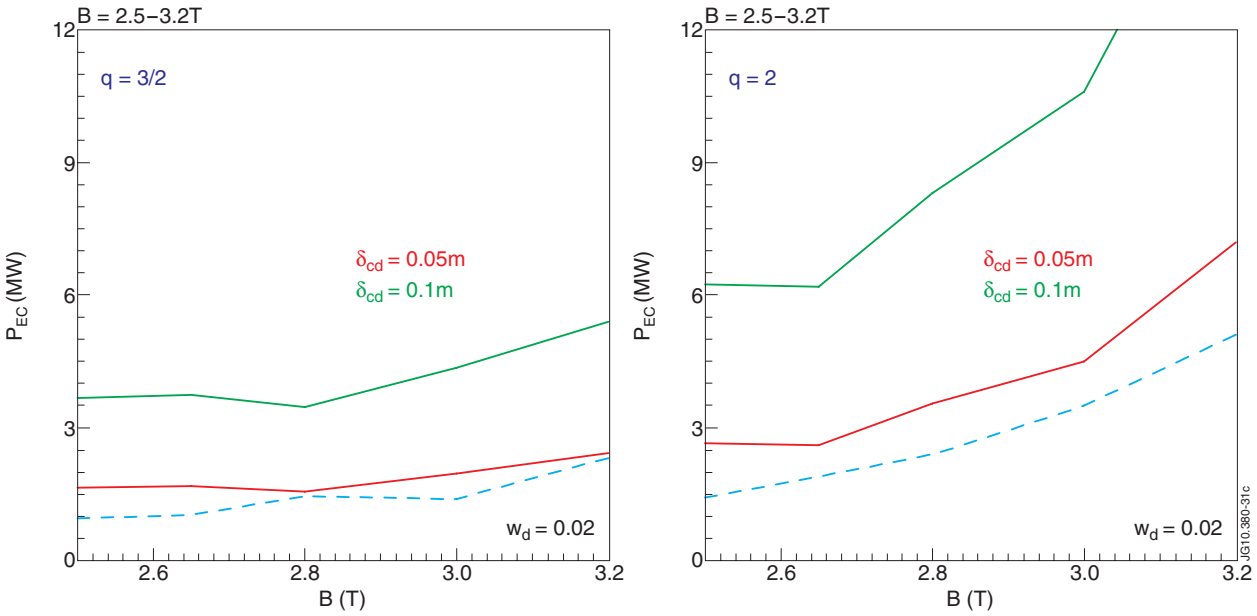


*Figure 9: EC power needed for suppression of the (3,2) mode (left) and of the (2,1) mode (right). Dashed line corresponds to the driven current widths dcd computed by beam-tracing; solid lines to the fixed values dcd = 0.05 and 0.1 m.*

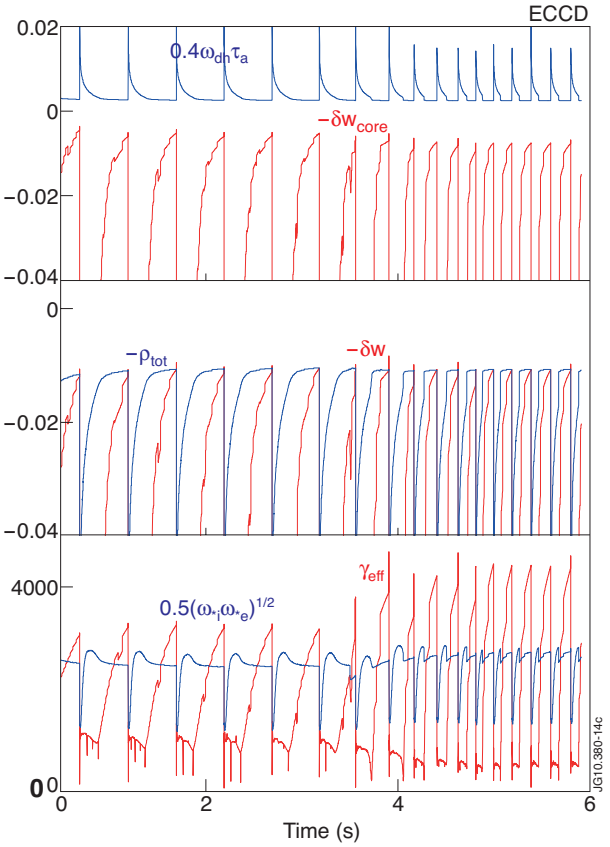


*Figure 10: Evolution of terms involved in the sawtooth stability criteria, calculated by the ASTRA Code. EC power is injected at t = 3.5s.*

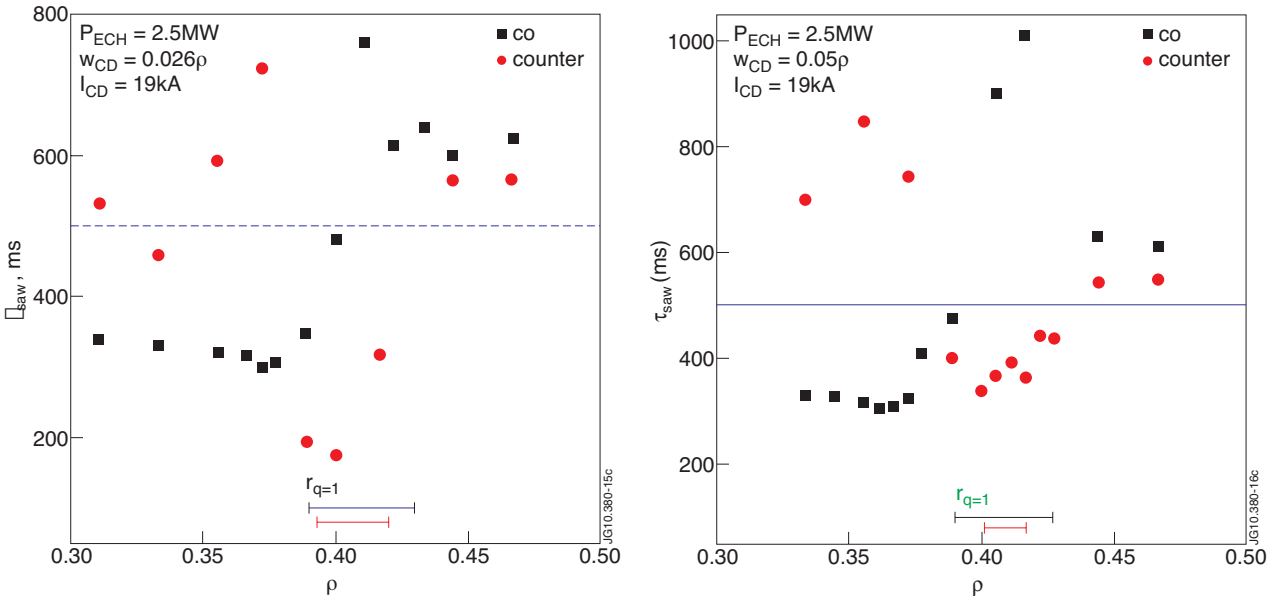


*Figure 11: Sawtooth period (ASTRA runs) versus ECCD radial location at ~1s after ECH switch on, for the conditions of the reference shot. Left: $w_{cd} = 0.025\rho$; right: $w_{cd} = 0.05\rho$.*

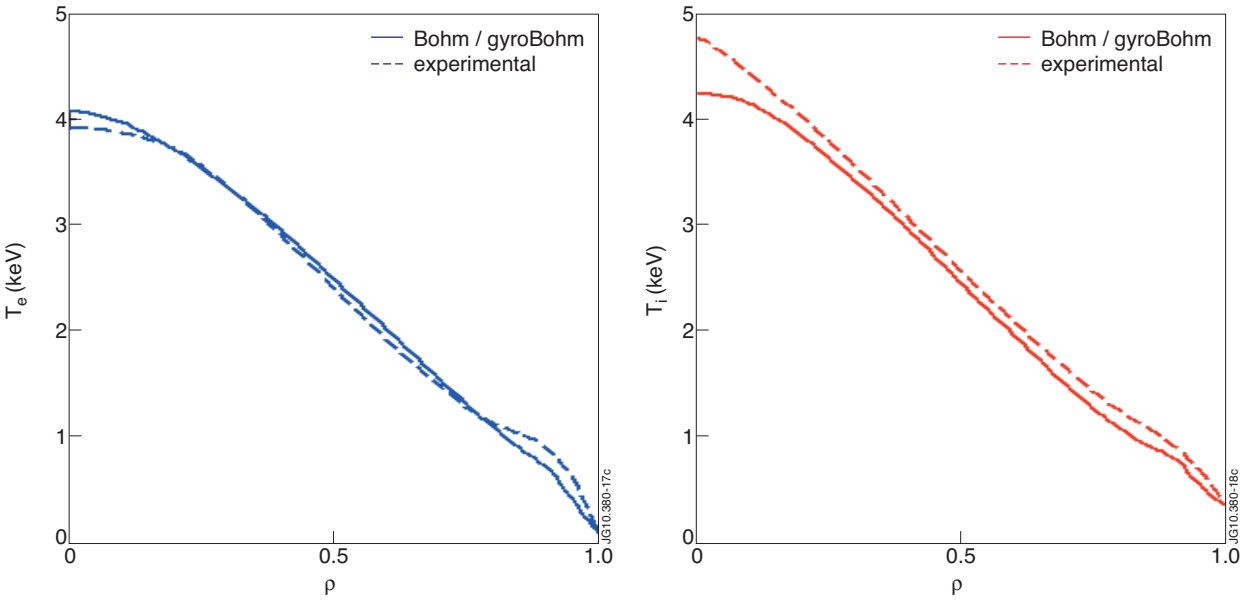


*Figure 12: Comparison of the electron and ion temperatures obtained by a predictive CRONOS simulation using the Bohm/gyro-Bohm transport model with the experimental fits, for Pulse No: 73344.*

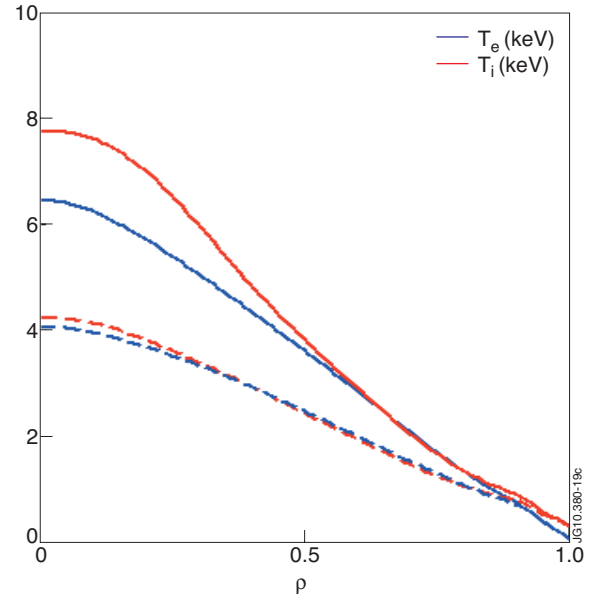


*Figure 13: Electron and ion temperature profiles at t = 21s, computed by predictive CRONOS simulations, for Pulse No: 73344 (dashed) and for $P_{NBI}$ = 32MW (solid).*

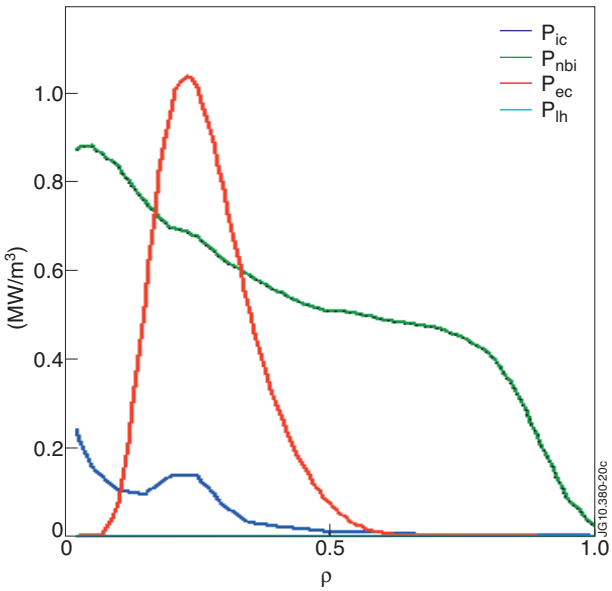


*Figure 14: Power deposition profiles, for $P_{NBI}$ = 32MW, $P_{IC}$ = 1.5MW, $P_{EC}$ = 10MW.*

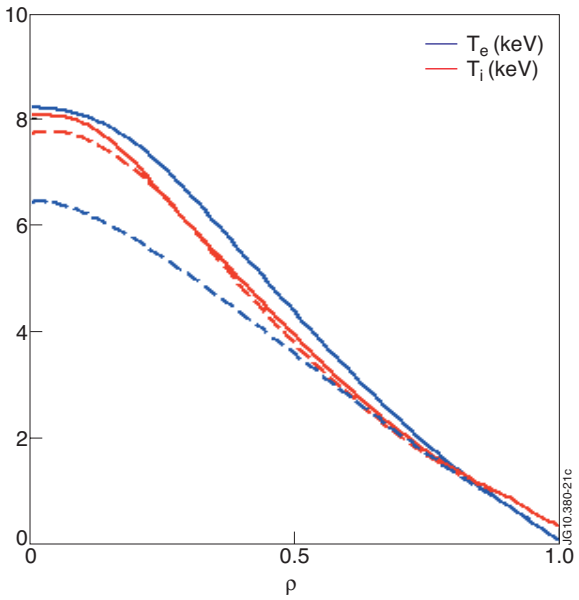


*Figure 15: Electron and ion temperature profiles at t = 20s, computed by predictive CRONOS simulations, for $P_{NBI}$ = 32MW. $P_{EC}$ = 0 (dashed) and $P_{EC}$ = 10MW (solid).*

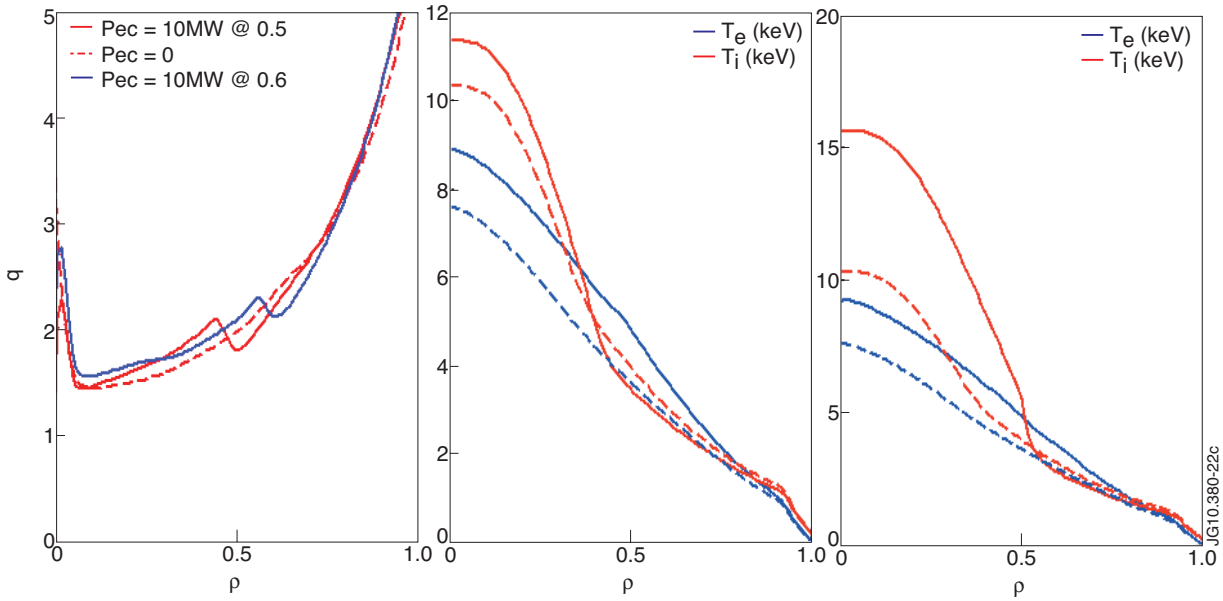


*Figure 16: Safety factor (left) and temperature profiles from predictive simulations of Pulse No: 77895, with the addition of 10MW ECCD. Temperatures for ECCD at ρ ~ 0.5 (middle) and ρ ~ 0.6 (right). Dashed lines: without ECCD; solid lines: with ECCD.*

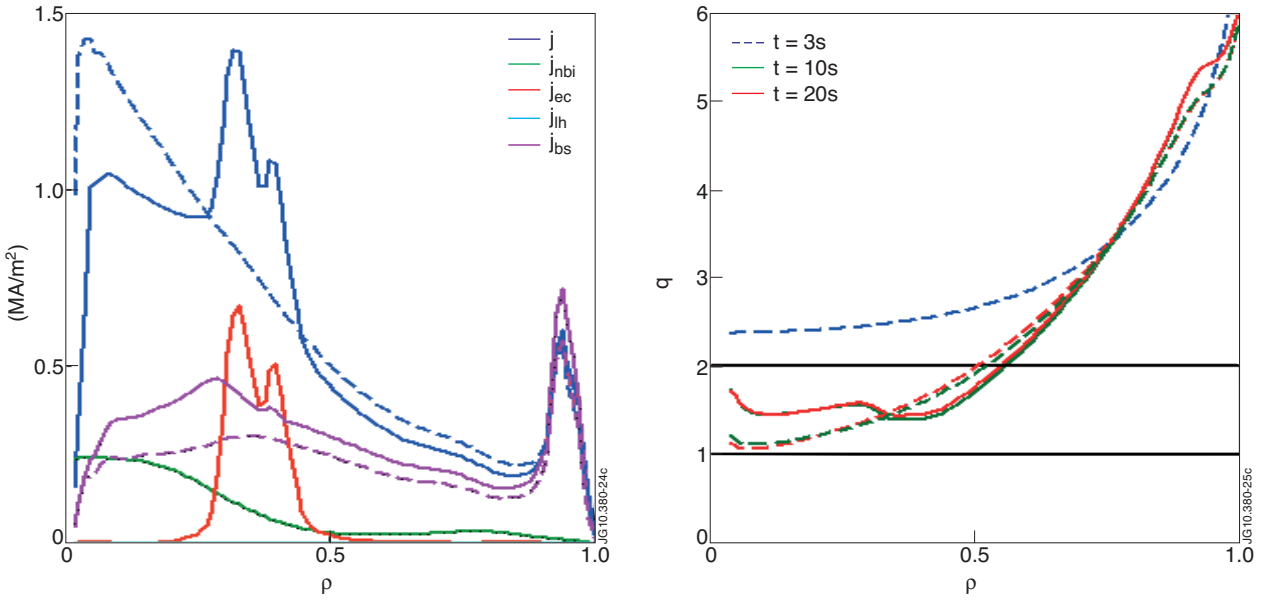


*Figure 17: Predictive CRONOS simulations of a JET hybrid-like scenario. Current density and current sources profiles with (solid) and without (dashed) ECCD (left). q profile evolution with (solid) and without (dashed) ECCD (right).*

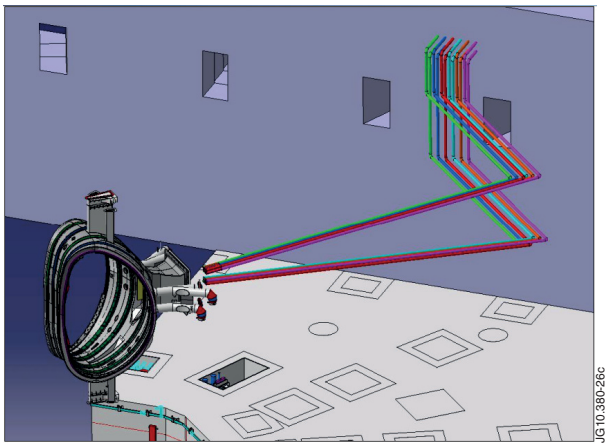


*Figure 18: A possible design option of the waveguide system in the JET Torus Hall, from the North wall to Octant 2.*

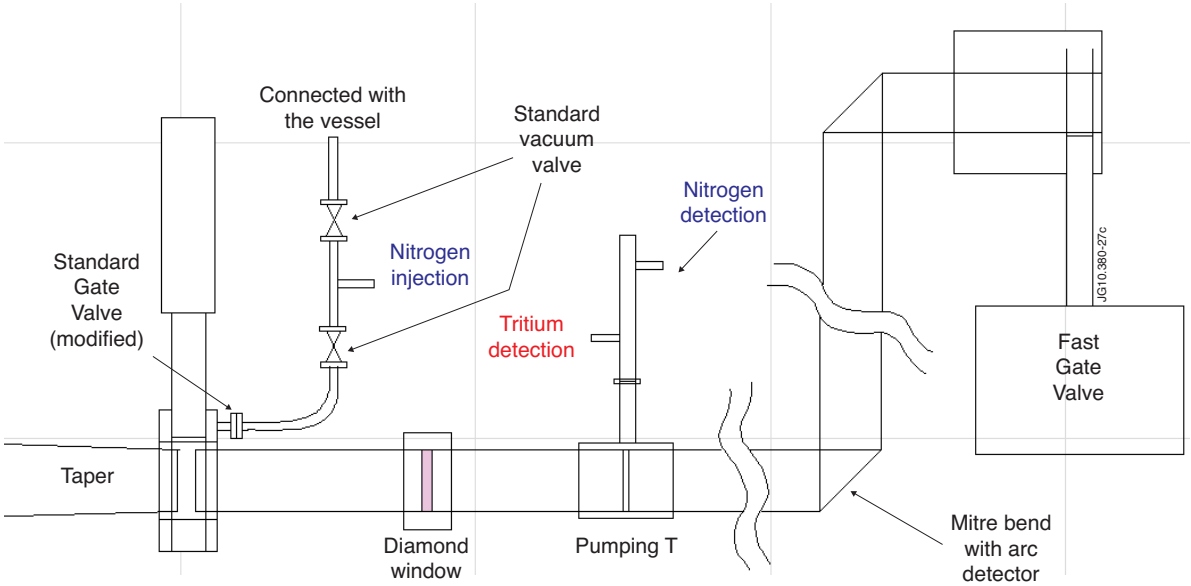


*Figure 19: Sequence of line components close to the launcher in the Torus Hall.*

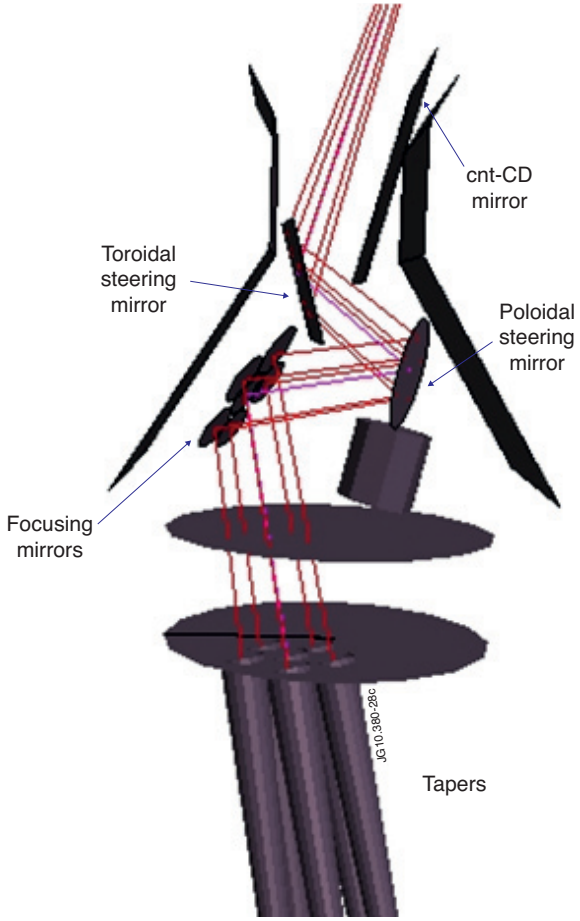


*Figure 20: Sketch of one of the two modules of the launcher.*

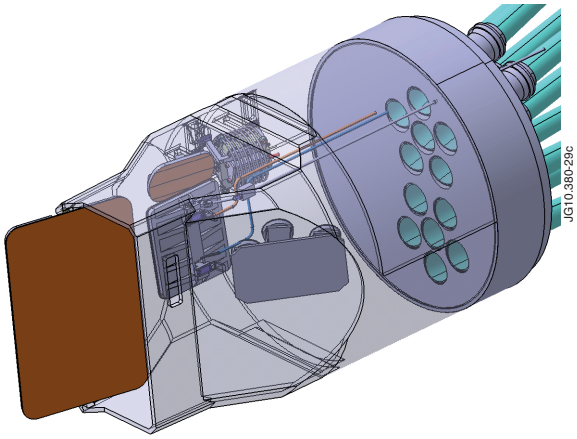


*Figure 21: Preliminary design of the JET launcher: outer structure of the plug-in unit, side (cnt-CD) mirror, focusing, poloidal and toroidal steering mirrors of the upper module.*

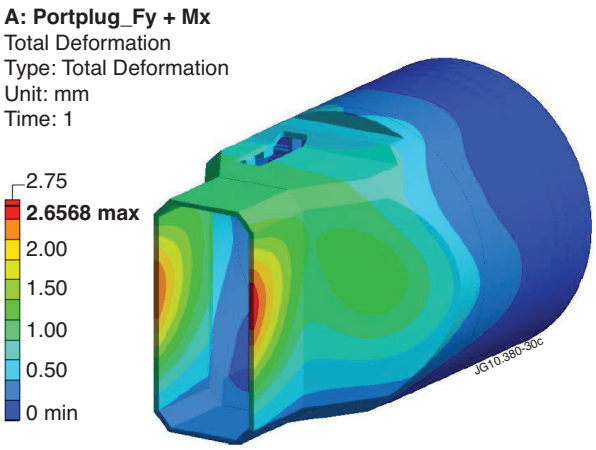


*Figure 22: Total deformation of the plug (in mm) due to electro-magnetic forces: 1MN force in the toroidal direction and a 1MNm moment in the radial direction (Finite Element simulation).*